PyCubed-Mini: A Low-Cost, Open-Source Satellite Research Platform

Neil Khera

CMU-RI-TR-23-47

August 08, 2023

The Robotics Institute
School of Computer Science
Carnegie Mellon University
Pittsburgh, PA

Thesis Committee:
Zachary Manchester, *chair*
Brandon Lucia
Jacob Willis

Submitted in partial fulfillment of the requirements for the degree of Master of Science in Robotics.

To my Nanu.

Abstract

Satellite development has become more accessible due to decreasing launch costs and shrinking hardware. However, the expenses associated with pre-built satellite kits remain high, making it difficult for student and hobbyist teams to participate. The lack of standardized satellite hardware and software further adds to the challenge, as small teams invest time and resources in recreating fundamental components instead of focusing on innovation.

To address these challenges, we present PyCubed-Mini: an open-source 1p PocketQube satellite research platform designed for affordability and user-friendliness. By utilizing readily available components and simple 3D-printed structural elements, the platform significantly reduces the entry barriers, making it accessible to universities, high schools, and individuals eager to engage in space exploration and pursue their research interests. Powered by CircuitPython, a Python-based development environment for embedded systems, PyCubed-Mini facilitates contributions from newcomers without limiting the possibilities for advanced research.

This thesis outlines the hardware design of the PyCubed-Mini platform, emphasizing the considerations made to ensure simplicity and cost-effectiveness. Additionally, we have developed a suite of open-source testing apparatus that allow comprehensive satellite testing on Earth, including long-range communications, solar charging, power testing, mechanical vibration testing, and day-in-the-life simulations. This testing framework will be a valuable resource for other satellite programs, reducing development and testing time.

PyCubed-Mini builds upon the legacy of the PyCubed 1U CubeSat motherboard, which has flown on three previous missions. The platform incorporates reliable hardware design practices, including novel serial bus protection circuitry and radiation testing data for commercial-off-the-shelf (COTS) components.

The PyCubed-Mini platform represents a significant step towards democratizing space exploration and supporting innovation in the satellite development community. Removing financial barriers and simplifying hardware and software integration will empower students and hobbyists to contribute to space research and advances in space technology.

Acknowledgments

I would like to thank Professor Zachary Manchester for his guidance and support over the past year-and-a-half that I have worked with him on the PyCubed-Mini project. Professor Manchester's passion for space exploration - a field that has fascinated me since childhood - and his immense knowledge about seemingly everything, has been incredibly inspiring. Thanks for giving me the chance to play with some seriously cool toys (and learn a lot while doing it)!

Of course, I would like to thank my family. This thesis has been dedicated to my *Nanu* (grandfather), who did so much for everyone he met, and whom I miss every day. I would also especially like to thank my parents for their unconditional love - even when I don't call as often as they'd like.

A special thanks to Jacob Willis for not only being part of my thesis committee but also for being a great friend. Thanks for supporting and guiding me through this process, and for being kind when the stress would get the better of me.

There are so many more people to thank, so in alphabetical order of their last names: Elmer Ford, Jordan Ford, Katie Ford, Ali Guzel, Joe Iacobellis, Dr. Heather Jones, KJ Newman, Alvin Shek, James "Jim" P. Teza, Srinivasan Vijayarangan, Warren "Chuck" Whittaker, and Dr. William "Red" Whittaker.

An additional thanks to the folks at The Exchange - Dave, Mike, Heide, Justin, Pedro, and Rocco. Thanks for keeping me fed during the writing of this thesis and for the great conversations!

Funding

PyCubed-Mini was supported by grants from the Carnegie Mellon University Portugal Program, the NASA Small Spacecraft Technology Program, and the National Science Foundation.

Contents

When this thesis is viewed as a PDF, the page header is a link to this Table of Contents.

List of Figures

List of Tables

Chapter 1

Introduction

1.1 Small Satellites

The last two decades have witnessed a flurry of innovation within small spacecraft design, development, and deployment. The Federal Aviation Administration's Office of Commercial Space Transportation (FAA AST) classifies satellites based on their launch mass [13] (Table 1.1). Small satellites (or smallsats) are satellites of low mass and size, usually weighing under 1,200 kg. Satellites in the **Nano**, **Pico**, and **Femto** classes are especially popular among budget space programs for their low cost of development and launch.

Since being proposed in 1999, the CubeSat reference design quickly became the most popular standard for small spacecraft missions. The standard one-unit (1U) CubeSat has dimensions of 10 cm $\times$ 10 cm $\times$ 10 cm and a maximum launch mass of 2.0 kg [50]. Figure 1.1 shows an example of a typical 1U CubeSat. The CubeSat design aimed to enable students to design, build, test, and operate a spacecraft in space with capabilities similar to that of the first satellite, Sputnik.

CubeSat designs typically utilize commercial-off-the-shelf (COTS) hardware components. Additionally, their small size allows for shorter development and testing periods. They are often launched in multiples, taking advantage of excess payload capacity on launch vehicles. The standard means to simplify the process of mating a satellite with its launch vehicle and minimize risks to the launch vehicle and other payloads. These design decisions result in lower development and launch costs.

Class name	Launch Mass (kg)
Femto	< 0.1
Pico	0.1 to 1
Nano	1.1 to 10
Micro	11 to 200
Mini	201 to 600
Small	601 to 1200
Medium	1201 to 2500
Intermediate	2501 to 4200
Large	4201 to 5000
Heavy	5001 to 7000
Extra Heavy	> 7000

Table 1.1: Federal Aviation Administration's (FAA) satellite classes [13]

Since 2014, the NanoSats Database (www.nanosats.eu) has been actively tracking all small satellite launches from the following categories:

- All CubeSats from 0.25U to 27U. The largest launched being 16U.
- Nano-satellites from 1kg to 10kg.
- Pico-satellites from 100g to 1kg.

As of May 31, 2023, there have been 2286 NanoSat launches from 82 countries. Of these, 2105 or about 92% were CubeSats. Surprisingly, however, only 620 (or 27%) of these satellites originated at universities [30].

Figure 1.1: V-R3x: A 1U CubeSat nano-satellite developed by the Robotic Exploration Lab (RExLab)

1.2 Challenges

Despite their proliferation, small satellite missions originating at universities have historically experienced high failure rates. A study by Berthoud et al. (2019) [2] displayed that between 1999 and 2018, only 26% of academic programs achieved total mission success. 32.7% of university missions were complete failures, with satellites either dead-on-arrival at their orbit or failing soon after deployment - and achieving none of their mission objectives (Figure 1.2). For first-time programs, the failure rate is greater than 50%.

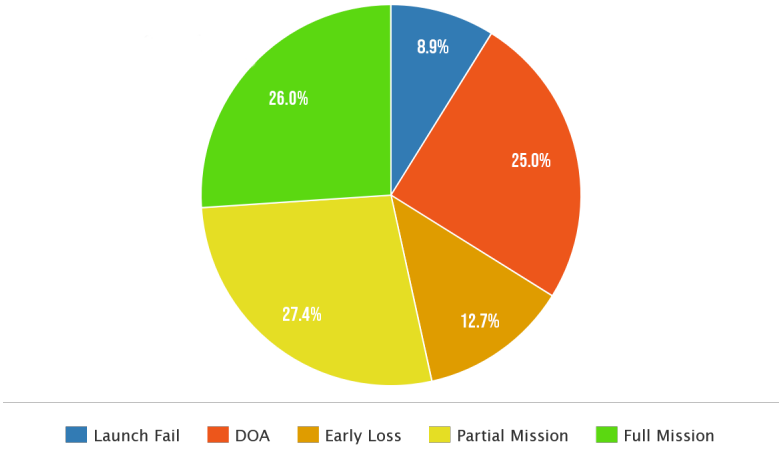

Figure 1.2: Mission status, all university-class missions (1999 - 2018)

University small satellite missions encounter several challenges that can impact their implementation and success. While university satellite missions offer valuable hands-on learning experiences for students and contribute to advancements in space technology and research, mission failures can be immensely discouraging and risk future funding possibilities. These challenges include:

1.2.1 Funding Constraints

Smallsat missions remain prohibitively expensive for all but the best-funded university programs. Pre-built satellite kits can cost tens of thousands of dollars upfront, while

developing custom hardware may require multiple rounds of iteration, which can deplete a constrained budget over time.

Factoring in launch prices, which for a single 1U CubeSat can be close to one hundred thousand dollars [39], it is clear why private companies, well funded through venture capital, dominate small satellite development.

1.2.2 Limited Expertise

Building a space-worthy satellite is a complex task and can be beyond the skill set of newcomers in the field. For example, satellites are typically embedded systems requiring C or C++ programming. New students may need to become more familiar with the complexities involved in such development. Refining these skills has a steep learning curve and may delay development.

A lack of familiarity with the larger space research community might mean that students spend time and energy learning and developing technologies that similar missions may have previously established.

1.2.3 Tight Schedules and Limited Launch Opportunities

Small satellite missions often fly as secondary payloads on scheduled launches, allowing developers to purchase excess payload mass at a relatively low cost. However, since priority is given to primary payloads, smallsat programs must often compress their testing schedules to meet inflexible launch dates or risk not flying at all.

Acquiring launch opportunities for smallsats can be challenging in general. Universities may have to wait for long periods for a suitable launch. Obtaining approval from regulatory agencies may be challenging and require design updates or prolonged validation. Some missions may experience delays even after delivering their satellite hardware to a launch provider, increasing the risk of satellite degradation during storage.

1.2.4 Testing and Validation

The primary reason for small satellite failures is insufficient testing prior to launch [52]. As mentioned, university satellite missions typically employ low-cost COTS

components not designed for the harsh environmental conditions of space — extreme temperatures, vacuum environment, high radiation levels, and micro-gravity.

Satellite designs, especially those with custom hardware, require extensive testing and verification to ensure mission success. Approximately one-third to one-half of the overall mission schedule should be allocated to integration, verification, and testing [52]. Essential tests include thermal vacuum, RF compatibility, deployment, hardware-in-the-loop, and software testing. However, universities may have limited access to space emulation facilities and hardware testing equipment.

1.3 Improving Accessibility

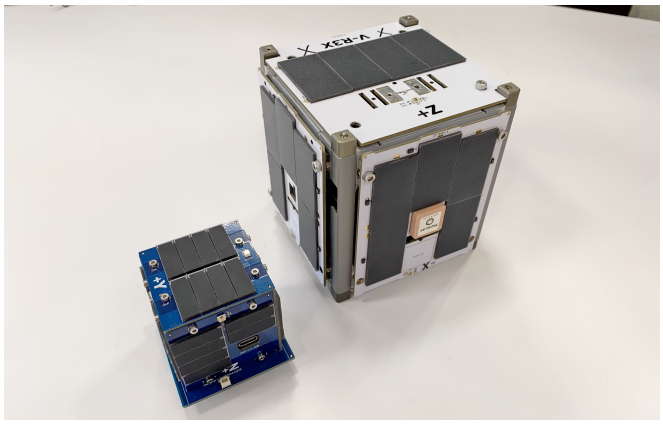

Figure 1.3: A 1p PocketQube (left) next to a 1U CubeSat (right)

Bob Twiggs, co-creator of the CubeSat standard, developed the PocketQube pico-satellite standard in 2009 to help universities worldwide build space science and exploration platforms [49]. The standard one-unit PocketQube (called a 1p PocketQube, as shown in Figure 1.3) with dimensions of 5 cm × 5 cm × 5 cm, and a maximum launch mass of 250 grams, is one-eighth the size and mass of a 1U CubeSat [36]. Being even lower cost to develop and launch than CubeSats, the PocketQube standard seems to be an attractive avenue for the future of smallsat development.

However, PocketQubes have not amassed the same popularity as CubeSats. As of May 31, 2023, only 59 PocketQube satellites have been launched, which includes larger variations of the standard, such as 1.5p, 2p, 2.5p, 3p, and 6p satellites [30]. Unlike

the PC/104 standard for CubeSat avionics boards, PocketQubes lack standardized hardware. They also exhibit reduced functionality relative to CubeSats, owing to their extreme physical constraints — for example, usually lacking any form of attitude determination and control system (ADCS). Additionally, commercial PocketQube kits remain prohibitively expensive to many — bare-bones kits costing upwards of twenty-thousand dollars.

Thus university programs are more likely to proceed with a well-established and capable CubeSat-based satellite design.

1.4 Our Work

We want more universities to build satellites and contribute to space research. Importantly, we want these universities to achieve full mission success.

In this thesis, we present the PyCubed-Mini 1p PocketQube satellite development platform (Figure 1.4), which has been in development at Carnegie Mellon University's Robotic Exploration Lab (RExLab) for the past 1.5 years. We follow the principles of **Open-Source**, **Low-Cost**, **Easy-to-Develop**, and **Extensively Tested** design to make small spacecraft development simple and accessible.

By doing so, we wish to standardize and establish the PocketQube standard on the same level of popularity as the CubeSat standard. We believe that our satellite design will offer a capable platform for not just university programs but will be accessible enough to be used even by dedicated high-school teams.

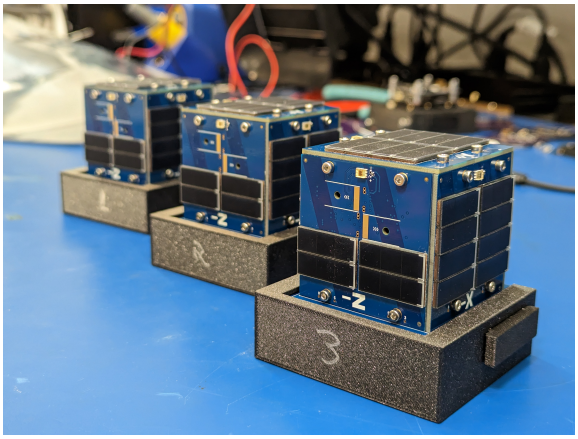

Figure 1.4: Three PyCubed-Mini PocketQube satellites

PyCubed-Mini features a simple mechanical design, incorporating 3D-printed parts and basic metric hardware, making it cost-effective yet resilient. It does not rely on any precision-manufactured components. The structure has been vibration-tested and is verified to survive the intense forces experienced by spacecraft during launch.

While designing the satellite's avionics system, we assessed performance, cost, and robustness. Prior work from our lab on open-source satellite hardware - namely the PyCubed board for CubeSats - gave us radiation performance data for several low-cost commercial-grade electronic components. We used this knowledge to inform our selection process for the mission-critical components onboard PyCubed-Mini.

PyCubed-Mini runs CircuitPython - a lightweight Python runtime for embedded systems. CircuitPython has been designed to be extremely simple and beginner friendly. It is cross-compatible with a standard Python implementation, extensively evaluated with unit tests, software-in-the-loop tests, and real-world tests, and boasts flight heritage onboard the KickSat-2 and V-R3x CubeSat missions. In keeping with our design principles of accessibility and ease of use, all our CircuitPython drivers, firmware, and flight software are fully documented and open-source.

We want PyCubed-Mini to be not only accessible but also capable. We have equipped our satellite with unique technologies unprecedented on a satellite of this scale. For example, we incorporate a magnetorquer-only attitude control system for full 3-axis control of the satellite. An Earth-observing camera module, coupled with a high-performance Computer Vision (CV) processor, has been integrated to achieve pico-scale machine vision capabilities in space.

Finally, PyCubed-Mini goes beyond solely a satellite design but aims to be an entire satellite development platform. We have created several pieces of supporting hardware, such as a ground station unit and testing devices, to verify the satellite's power, communication, and attitude control systems. Like the satellite, these designs are completely open-source and optimized for low cost and ease of use.

The PyCubed-Mini platform will facilitate future PocketQube launches by lowering the barrier of entry, streamlining satellite development, reducing iteration and turnaround times, and cutting costs - thereby accelerating innovation in small-satellite research. We have prioritized optimizing and thoroughly documenting the manufacturing, assembly, and programming processes. The platform has undergone full integration, verification, and extensive testing to confirm its flight readiness.

PyCubed-Mini will embark on its maiden space voyage in late 2023. Another launch will follow soon after. A space mission represents the ultimate validation of our design, and we eagerly anticipate these upcoming launches.

We commence this thesis with a comprehensive exploration of the satellite hardware design in Chapter 2 - delving into design considerations, feature requirements, and compromises that have led to our current designs. Subsequently, we discuss manufacturing, assembly, and integration practices, followed by an in-depth discussion of testing methodology, equipment, and processes in Chapter 3. Finally, we touch upon future work and potential areas for further development in 4.

Chapter 2

Hardware Design

This thesis section will provide an in-depth discussion of PyCubed-Mini's hardware design as a 1p PocketQube satellite. We divide our discussion along the lines of six classical spacecraft subsystems: Structural design, power, avionics design and computing, communications, attitude determination and control system (ADCS), and the payload - which, in the case of our satellite is a machine-vision camera system.

We aim to elaborate on the design requirements, considerations, merits, and compromises - to adhere to our design principles of building an open-source, low-cost, easy-to-use satellite research platform.

2.0.1 Nomenclature

The axes convention and nomenclature used while defining the PocketQube standard are represented in Figure 2.1.

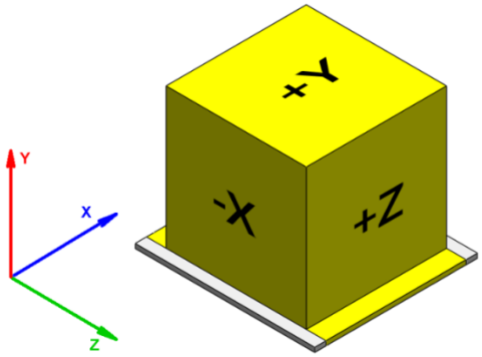

Figure 2.1: PocketQube Axis Specification [36]

Solar-panels mounted on each of the six faces of our PocketQube satellite are designated and labeled with their corresponding axis: +/-X, +/-Y, +/-Z, as expressed above (See, solar panels labeled -Z and -X in Figure 1.4). We will adopt this convention and nomenclature for the rest of this thesis.

2.1 Structural Design

We begin our exploration of PyCubed-Mini's hardware by delving into its structural design. Our primary goals during the structure design phase were simplicity, low cost, low mass, rigidity and strength, and ease of manufacturing and assembly.

2.1.1 Pre-Design

Due to the PocketQube standard's limitation of a maximum launch mass of 250g, we faced constraints in the complexity of our mechanical structure. It was essential to select low-mass materials while ensuring they possessed the necessary structural rigidity. Moreover, the materials selected had to meet the out-gassing limits enforced by space launch providers.

Metals have high rigidity, are homogeneous and isotropic, and typically exhibit low out-gassing in a vacuum. These properties make them ideal materials for spacecraft structures. CubeSats, for example, usually employ a metal chassis frame (Figure 2.2) to form the structural skeleton of the satellite. Avionics circuit boards are then fixed within the chassis, and solar panels are mounted on each face of the cubic structure.

These are precision-manufactured structures comprising low-mass, space-grade metal alloys of Aluminum or Titanium [33].

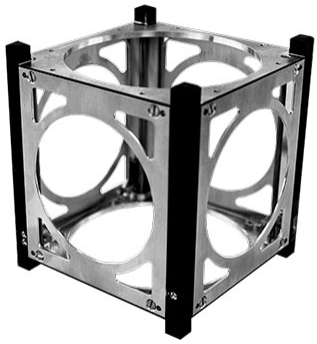

Figure 2.2: Precision manufactured 1U CubeSat chassis. *credit: AAC Clyde Space*

While a 1U CubeSat chassis has a relatively low mass of around 100 grams, or 5% of its maximum launch mass, on the PocketQube-scale, a metal chassis would contribute a significant fraction of the satellite mass. The commercial PocketQube kit manufactured by Alba Orbital (Figure 2.3) has a chassis mass of 69 grams or approximately 28% of the entire PocketQube mass budget [34].

Furthermore, adopting such a structure would necessitate precision milling and manufacturing through complex and expensive CNC processes. To remain consistent with our design principles of low cost and ease of manufacture, we designed PyCubed-Mini's mechanical structure to be composed solely of 3D-printed parts manufacturable on conventional printers and simple COTS hardware.

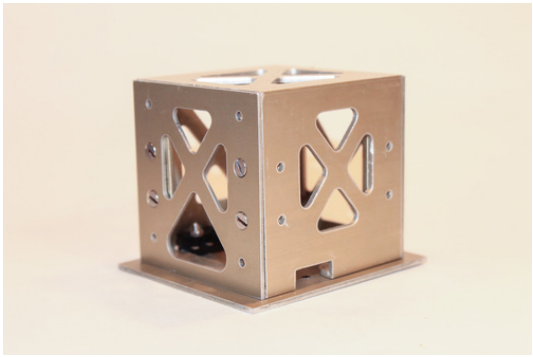

Figure 2.3: Chassis from Alba Orbital's 1p PocketQube kit [34]

2.1.2 First Iteration

We first devised a three-part 3D-printed structure with the following configuration: a hollow ring-like component (nicknamed the "donut") intended to house the satellite's batteries and two perpendicular "rails", with threaded heat inserts installed as mounting points for the solar panels. The rails featured internal grooves to slide-fit the avionics boards inside the satellite.

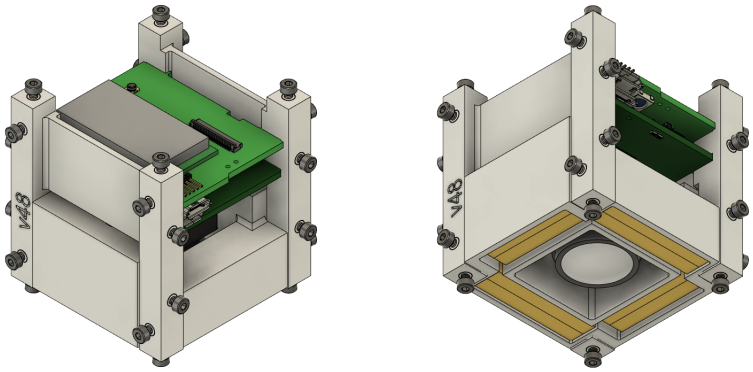

Figure 2.4: Initial mechanical design for PyCubed-Mini. Top-view (left), and bottom-view (right)

This design presented particular challenges. Due to the use of lightweight plastic, the structure walls needed to be quite thick to be mechanically stable, thereby reducing the available internal volume of the satellite. Additionally, the battery "donut" occupied over one-third of the satellite's internal volume and required dividing the battery storage into eight 150mAh Lithium-Polymer (LiPo) cells (bottom-view Figure 2.4).

LiPo cells must have their voltages balanced before being connected in a parallel circuit. If unbalanced, a higher-voltage battery could drive a large reverse current onto a lower-voltage battery, potentially causing the battery to overheat and explode. The greater the number of cells, the more tedious, laborious, and time-consuming the task of balancing battery voltages becomes.

A reduction of available internal volume implies a reduction in the number and size of the avionics boards that can fit within the satellite. Due to the inherent imprecise tolerances associated with 3D-printed structures, the avionics boards held

by the rails fit poorly in their grooves, which is unsuitable for flight.

The lack of physical contact between the internal avionics boards and the solar panel boards means that electrical connections between boards had to be made through an unwieldy custom-designed flat-flex ribbon cable (Figure 2.5). Routing this cable within the confines of the satellite during assembly was extremely tedious, and minor updates to the structure or circuit-board designs required a redesign of the cable as well. As a result, this initial mechanical design was not modular.

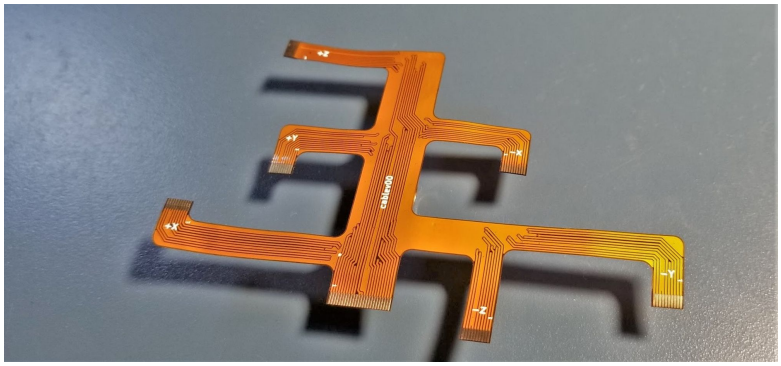

Figure 2.5: Custom flat-flex ribbon used in our initial structural design

2.1.3 Current Design

The PC/104 CubeSat standard for stacked internal circuit-board layout and connector selection facilitates modular electronics design [5]. We took inspiration from this standard to create the current version of our mechanical design and inter-board electrical connections. We leverage the rigidity and excellent mechanical tolerances of low-cost printed circuit boards (PCBs) to form a sturdy internal structure for the satellite and reduce wasted space by the previously voluminous 3D-printed components. This stacked-board design is displayed in Figure 2.6.

The circuit boards are spaced and secured with simple metric M3 standoffs. The +Y and -Y solar panels here form the top and bottom layers of the avionics stack. Internal to the +Y and -Y solar panels are fixed two ring-shaped 3D-printed parts (colored in grey in Figure 2.6). Threaded heat inserts are installed in these components to serve as mounting points for the four remaining solar panels. The updated mechanical structures can be prototyped in under 40 minutes using ordinary filaments on conventional 3D printers.

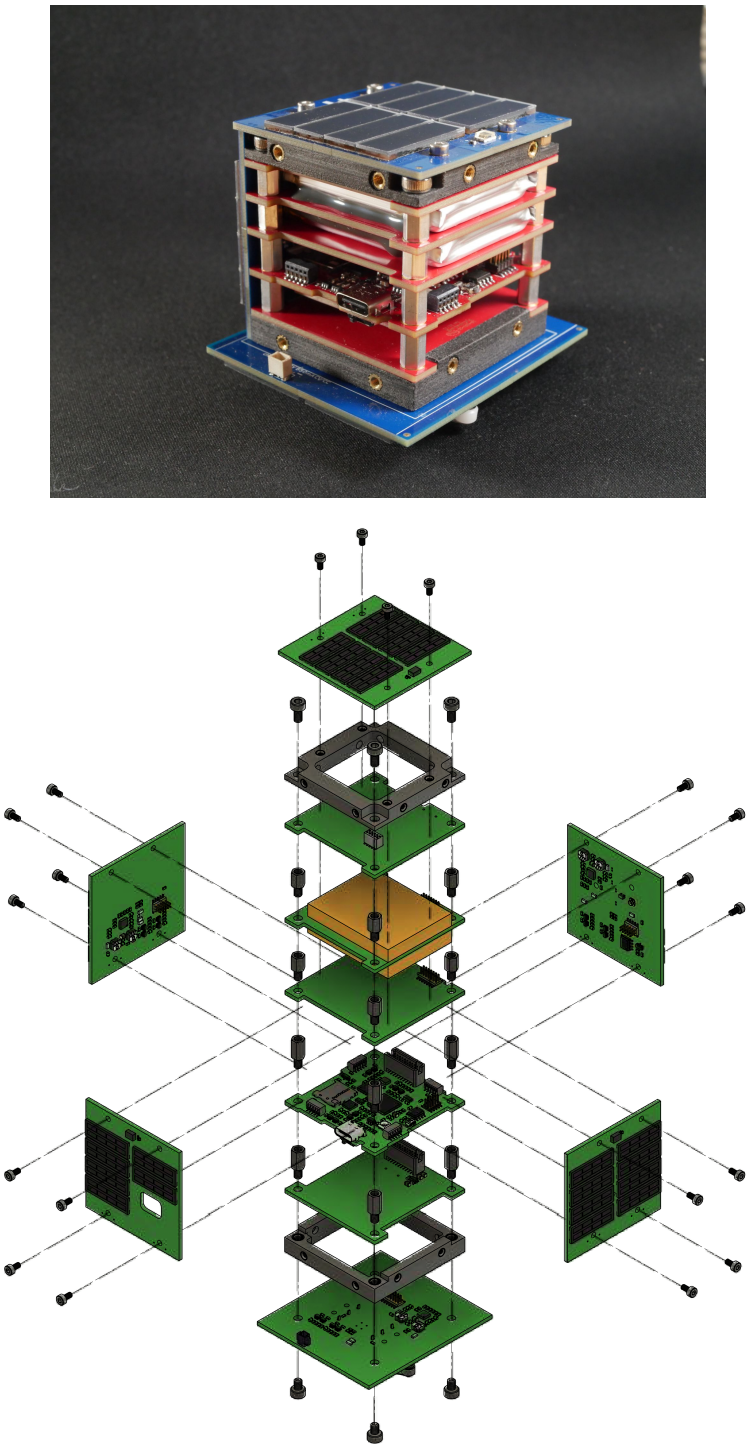

Figure 2.6: PyCubed-Mini mechanical structure (top) exploded view (bottom)

Avionics Boards

The stacked avionics design eliminates the need for the complex flat-flex ribbon cable for inter-board electrical connections. Like the PC/104 standard for CubeSats, electrical connections between the stacked avionics boards are made through pin header/socket board-to-board connections (Figure 2.7). Connections between the side-mounted solar panels and the avionics stack are made through right-angled pin header/sockets (Figure 2.8).

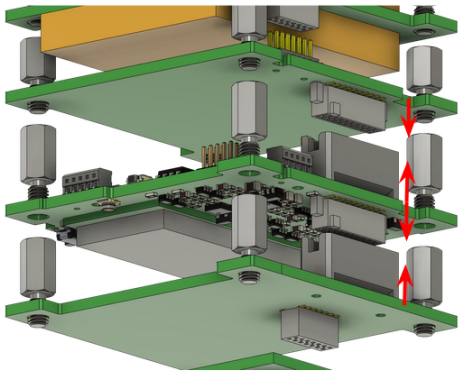

Figure 2.7: Avionics stack inter-board electrical connections

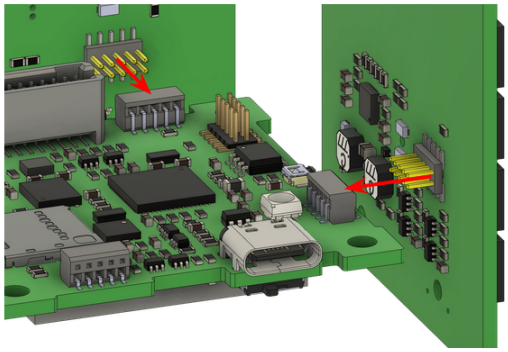

Figure 2.8: Solar panel electrical connections to the avionics stack

The increased internal satellite volume allows more avionics boards within the satellite - an increase from 2 to 5. Three of these boards additionally serve as structural components for the batteries, as discussed in the next section. The internal avionics stack of the PyCubed-Mini features the following boards from top to bottom:

- **top-batteryboard**: Top of the battery "sandwich". Top surface available for additional components in future designs.
- **middle-batteryboard**: Batteries are soldered to terminals on this board in a parallel circuit — one cell on each side.
- **bottom-batteryboard / Electrical Power Systems (EPS) board**: Bottom of the battery "sandwich". The bottom surface contains power monitoring circuitry.
- **mainboard**: Main processing board of the satellite. Primary microcontroller unit (MCU), sensors, coil drivers, and radio module.
- **cameraboard**: 5 Mega-pixel camera for space-observation. High-performance secondary MCU for machine-vision processing.

Furthermore, the size of the avionics boards is increased by 31% (Figure 2.9). Considering the two additional available surfaces from the new batteryboards, the surface area available for avionics components is increased by 96%

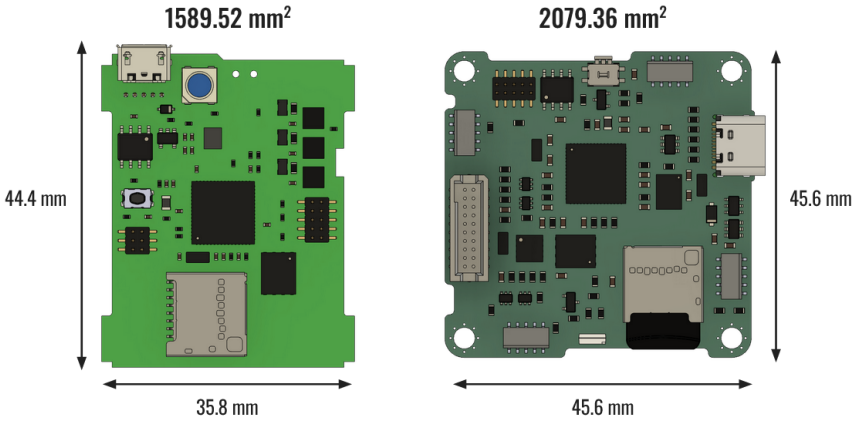

Figure 2.9: Avionics board sizes: Initial design (left). Current design (right)

The additional surface area enabled the integration of novel bus protection circuitry on each I2C and SPI component, protecting the satellite's serial communication buses. Furthermore, the minimum package size of passive components (resistors, capacitors, inductors) was increased to a 0603 imperial package (0.06" × 0.03") - aiding ease-of-manufacture. Optimizing the component selection and avionics design for ease of manufacture and assembly is discussed in detail later.

Batteries

LiPo batteries are available in two main package types: cylindrical cells in aluminum casings and flat pouch cells. While cylindrical cells offer increased mechanical stability, they are available in standardized packages only and have low energy density. On the other hand, pouch cells are available in various sizes and can be tailored to fit into the available space within a satellite. They also offer high energy density for their volume due to their lack of rigid housing.

We have opted for pouch cells for our satellite design, allowing us to maximize power capacity within the constrained confines of a PocketQube satellite. The increased power capacity enables the integration of more powerful components and increases the satellite's operation time.

As a result of the increased internal volume due to our structural redesign, we have been able to switch from 8 × 150mAh cells to 2 × 850mAh cells - reducing the number of batteries that must be balanced prior to installation and increasing our overall power capacity from 1200mAh to 1750mAh - a 41% improvement.

However, a critical concern associated with pouch cells is that the absence of a rigid structure can allow them to swell in the vacuum environment of space. Swelling could result in structural damage and potential rupture of the cells, which poses a severe risk to the integrity of our satellite. To address this, we have sandwiched the pouch cells between rigid PCBs in our avionics stack, constraining any potential swelling. This battery sandwich is displayed in Figure 2.10.

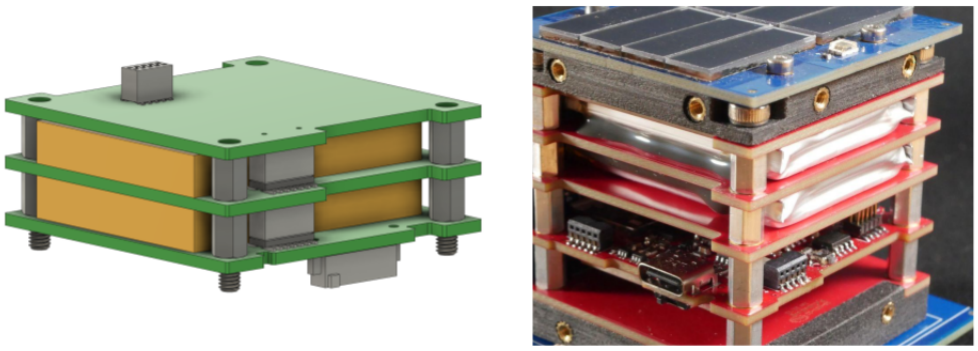

Figure 2.10: Pouch cells "sandwiched" between rigid stack PCBs

2.2 Power System

PyCubed-Mini is a solar-powered satellite. Due to the small physical size of the PocketQube standard, the satellite's power system must be devised to work efficiently within the constraints of limited power production due to the minimal surface area for solar panels, as well as limited power storage capacity due to the small internal volume available for batteries. Figure 2.11 presents a high-level block diagram of PyCubed-Mini's power system.

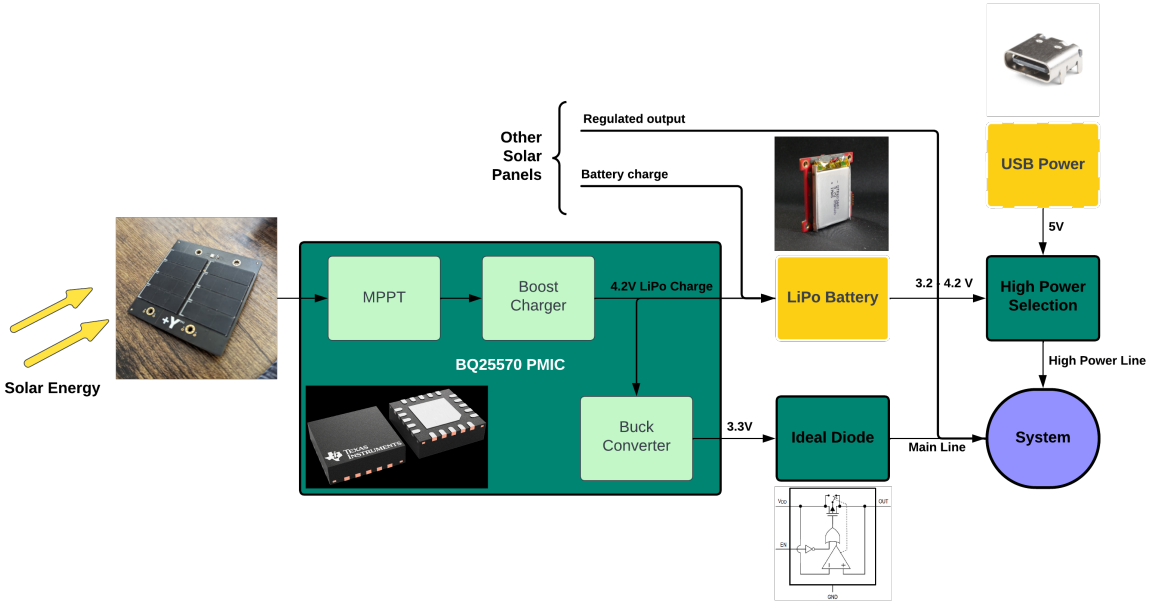

Figure 2.11: High-level block diagram of PyCubed-Mini's power system

Incident solar energy on the photovoltaic (PV) cells on the satellite's exterior produces a usable voltage. A power management integrated circuit (PMIC) harvests this input voltage and steps it up to charge the satellite's batteries. The PMIC also steps down power from the batteries to supply the satellite's main voltage line (3.3V) on which most components operate. The batteries directly power the high-power line that supplies components with higher power requirements. A source selection circuit allows the avionics boards to be preferentially powered via USB DC input, allowing board development without requiring full satellite integration.

We discuss the design of the individual components of the power system next.

2.2.1 Solar Panels

Solar panel PCBs comprise each face of the PyCubed-Mini satellite. Each solar panel accommodates 4 to 8 photovoltaic cells. We have chosen the KXOB25-05X03 monocrystalline cells manufactured by AnySolar Ltd for our current solar panel designs. These cells are COTS components, readily available as in-stock items from Digikey, and costing less than $3 per cell when purchased in bulk. The six solar panels cost approximately $200, which includes PCB fabrication and component purchasing.

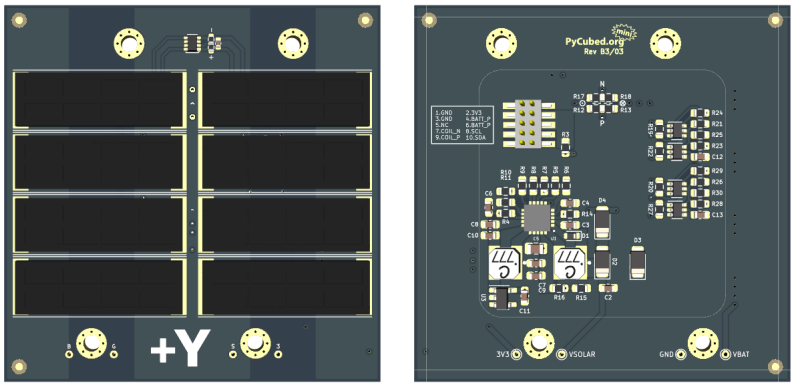

Figure 2.12: The +Y solar panel. External surface (left) and internal surface (right).

Each KXOB25-05X03 solar cell has an open-circuit voltage of 2.07V. On PyCubed-Mini, the typical arrangement of these cells is a 2-series-4-parallel (2s4p) configuration, resulting in a solar panel open-circuit voltage of 4.14V. At the point of maximum peak power (MPP), the solar cells have a voltage of 1.67V and an output current of 18.4mA, resulting in a maximum power production of 30.7mW per cell. Thus, a solar panel with eight cells can produce a maximum of 245.6mW of power [12].

The drawback of using COTS solar cells is that they typically exhibit lower efficiency than state-of-the-art alternatives. AnySolar's cells have a rated efficiency of 25%. In comparison, Spectrolab's high-efficiency TASC cells, used on the commercial PocketQube solar panels from Alba Orbital, have a rated efficiency of $> 30\%$. These panels have a maximum power production of 368mW - about 50% higher than ours. On the other hand, this kit of just five solar panels costs more than $6000 [35]. We decided this loss in efficiency was a worthwhile compromise for the gained cost and accessibility advantage.

2.2.2 Maximum Power Point Tracking (MPPT)

Photovoltaic (PV) cells exhibit a complex relationship between their operating environment and the power they generate. Under specific conditions, these cells have a singular operating point at which the values of current (I_{mpp}) and voltage (V_{mpp}) enable the maximum power output. These values correspond to a particular 'characteristic' load resistance, equal to V_{mpp}/I_{mpp} as specified by Ohm's law. Figure 2.13 displays this relationship between current and voltage.

The characteristic load resistance is a dynamic quantity that changes depending on the illumination level, temperature, and cell condition. Any lower or higher load resistance will result in a reduction in power output from the cell. Maximum power point trackers utilize control circuits or logic to identify this point [54].

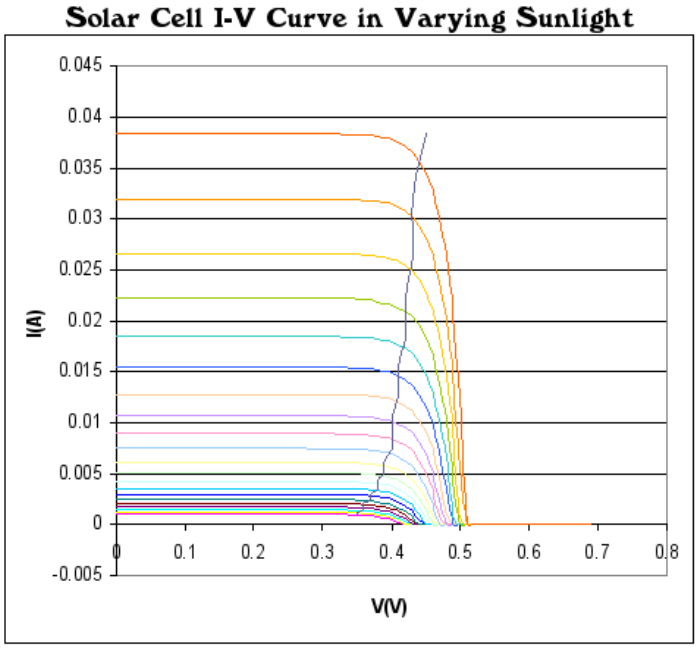

Figure 2.13: Photovoltaic solar cell I-V curves. A line intersects the knee of the curves, which represents the maximum power transfer points [54]

AnySolar recommends Texas Instruments (TI) BQ25570 ultra-low-power harvester IC for efficient power harvesting from the KXOB25-05X03 solar cells. The BQ25570 IC is equipped with Maximum Power Point Tracking, allowing it to dynamically

vary the load characteristic (impedance) of a system to keep photovoltaic cells at or near their point of maximum power production [24]. The MPP voltage of PV cells is typically 75-80% of their open circuit voltage. For our solar panel configuration, the MPP voltage is approximately 3.34V.

2.2.3 Power Harvesting and Storage

The BQ25570 uses power harvested from solar panels to charge the satellite batteries. This IC can efficiently extract nano-watts of power from the solar cells, making it capable of harvesting even power generated by partially shaded solar panels. Each solar panel on the satellite is equipped with its own BQ25570 IC and associated circuitry to optimize power harvesting.

Since the charge voltage of Lithium Polymer (LiPo) batteries is 4.2V, the IC contains a boost charging circuit to step up the input voltage from the solar panels to the battery charging voltage.

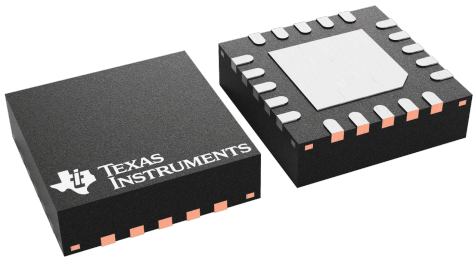

Figure 2.14: BQ25570 PMIC from Texas Instruments. Harvests solar panel power, charges batteries, and supplies the satellite's main 3.3V line

PyCubed-Mini features exceptional power storage capabilities, owing to its 1700 mAh capacity implemented as 2 × DTP603443 LiPo batteries connected in parallel (Figure 2.15), for a nominal battery voltage of 3.7V and a full charge voltage of 4.2V. These COTS batteries are available from the hobbyist electronics supplier SparkFun. They include built-in protection circuitry, safeguarding against over-charge, over-discharge, over-current, short circuits, and electrostatic discharge (ESD) events.

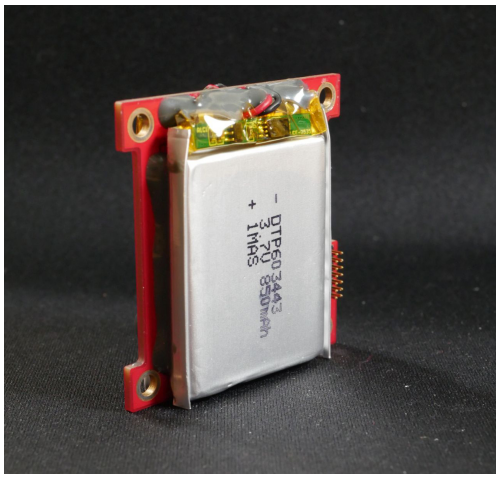

Figure 2.15: LiPo cells installed on a middle-batteryboard (second cell not visible)

The -Y solar panel has disconnect switches that isolate the battery terminals from the satellite's power system. These switches are mechanically depressed in a PocketQube deployment pod (Figure 2.16), disconnecting the batteries and keeping the satellite powered off. Upon deployment in space, the switches reset, connecting battery power, turning the satellite on, and initiating its operation.

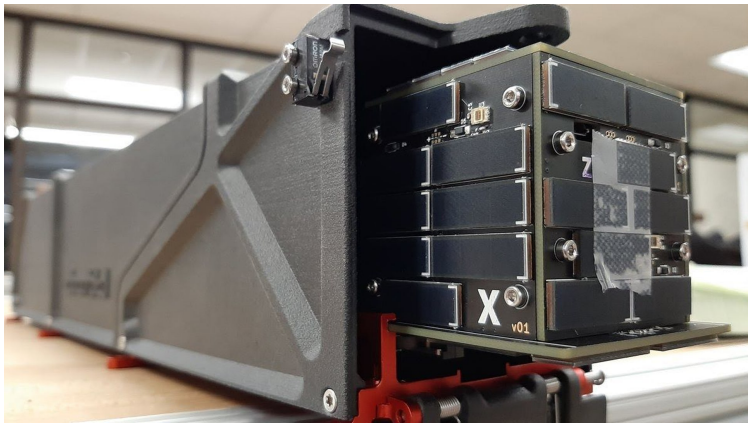

Figure 2.16: An early iteration of PyCubed-Mini being test-fit into an Alba Orbital deployment pod

2.2.4 Main Power Line

In addition to charging the batteries, the BQ25570 incorporates an output buck converter that steps down the battery voltage to an adjustable level, which we have set to 3.3V based on the voltage specifications of other components. Each PMIC allows a maximum current output of 110 mA. The 3.3V outputs from all the solar panels are tied together, allowing a maximum current draw of 660 mA on the satellite's main power line. This line powers the mainboard MCU, most of the sensors on the mainboard, the EPS board, and the light sensors on the solar panels. Due to the nature of a buck converter, this also means that when the battery voltage falls below 3.3V, the main line (and effectively the entire satellite) will turn off.

Since the 3.3V outputs are all tied together, we must add a forward-biased diode on each output to prevent reverse current on the ICs (Figure 2.17). Typical Schottky diodes have a significant forward voltage drop, around 500mV, corresponding to a nearly 15%

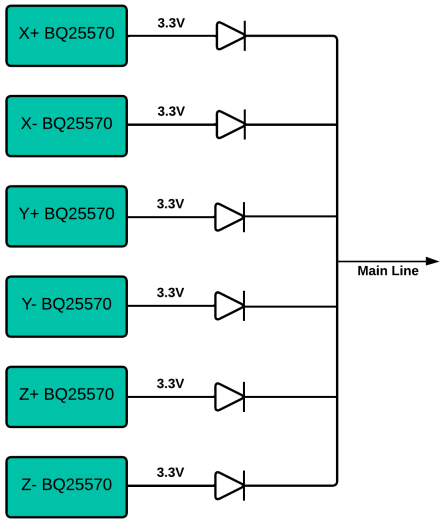

Figure 2.17: Simple power OR-ing circuit

We use Analog Devices' MAX40200 1A ideal diode instead of a Schottky diode. Ideal diodes are P-channel MOSFETs configured to function as diodes, offering a forward voltage drop approximately an order of magnitude lower than Schottky diodes

(Figure 2.18). Unlike regular diodes, which have a relatively constant forward voltage over a wide range of currents, ideal diodes behave more like resistors exhibiting an increasing forward voltage with rising current draw. For a maximum current of 110mA per diode, we can estimate the maximum voltage drop across the MAX40200, from its datasheet, to be around 20mV, which is more acceptable [11] [8].

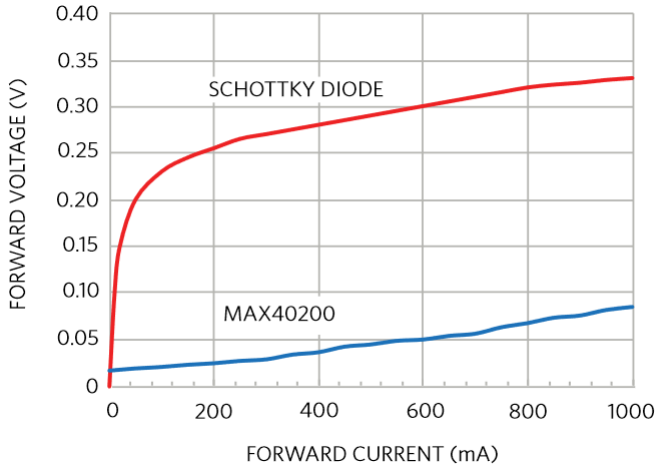

Figure 2.18: MAX40200 vs. Schottky Diode: Forward Voltage / Current Comparison

Both the battery charger and buck converter are switching power regulators which boast high efficiency, up to 93% under typical conditions [24]. Switching regulators have drawbacks of requiring many external components and causing increased electronic noise. Consequently, careful consideration is required when laying out the circuit components and routing data lines. We follow TI's recommended PCB layout guidelines in the BQ25570 datasheet to ensure optimal performance.

2.2.5 High-Power Line

A high-power line powers components with increased power demands. This line is typically connected directly to battery power. Avionics boards with high-power components like the mainboard and cameraboard feature specialized power-selection circuitry. The selection circuit uses the LTC4412 low-loss power path controller [10] (Figure 2.19), which allows the high-power line to be selectively powered by USB 5V supply when it is present. This feature is beneficial during development and testing, allowing powering of the boards outside the satellite system.

A low dropout (LDO) voltage regulator on the mainboard generates the 3.3V main line when operating on USB power. While LDOs are typically lower efficiency than switching buck converters, they are much simpler to integrate, feature little external circuitry, have a small PCB footprint, and have much lower noise on their output. These features are advantageous on the somewhat cramped mainboard since we are not concerned about power loss on a USB line.

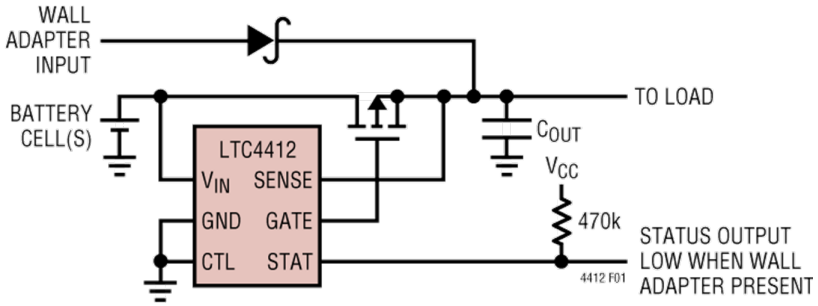

Figure 2.19: LTC4412 Application Circuit [10]

Since the high-power line may operate at various voltage levels, we verify that components powered by it are tolerant to and functional at the 4.2V nominal battery voltage, 3.3V minimum battery voltage, and 5V USB voltage.

2.2.6 Electrical Power Systems (EPS) Board

The bottom batteryboard that forms the lower mechanical component of the battery sandwich also serves as the EPS board on our satellite (Figure 2.20). The current revision incorporates a current-sensing IC - the INA219 by Texas Instruments - an I2C-based sensor built around a high-precision analog-to-digital converter (ADC). The IC measures the voltage drop across a known resistance (called a shunt resistor) and, as such, can accurately estimate current draw with a low measurement error of +/-0.5% [23].

Current from the batteries flows through a series shunt resistor towards the rest of the satellite system. The selected resistance value affects the range and resolution of the current sensor. A higher resistance allows the sensor to measure higher currents but results in a more significant voltage drop on the battery line and power loss in the form of heat. We have selected a 0.04 ohm power resistor (Part no. SMS-R040-1.0)

in a 1% tolerance, large 2516 (0.25" × 0.16") SMD package. This resistance enables a maximum sensing current of 8A with a resolution of 2mA, which works well with our expected nominal and maximum current draws.

In certain instances, such as during antenna deployment, a large current draw may generate significant heat at the shunt resistor. The selected power resistor is specially designed to withstand high temperatures, with a rated thermal range of up to 170 degrees Celsius [51]. Additionally, the resistor package features large pads that efficiently dissipate heat into the copper layers of the PCB.

Considering future revisions, we plan to enhance the functionality of the EPS board to improve power monitoring and management on the PyCubed-Mini satellite. We discuss potential additions and improvements to the power system design in the final chapter of this thesis.

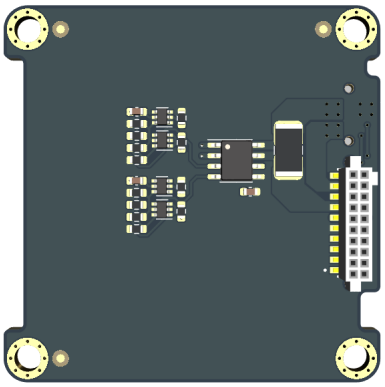

Figure 2.20: Bottom-batteryboard / EPS board -Y surface

2.3 Avionics Design and Computing System

2.3.1 Informed Avionics Design

PyCubed-Mini's avionics design carries the legacy of the full-sized PyCubed mainboard for CubeSats towards building open-source and user-friendly satellite hardware. Designed by RExLab in 2019, the PyCubed board has since gained immense popularity within the smallsat community [18]. PyCubed has proven its space-worthiness by serving as the motherboard for the successful KickSat-2 and V-R3x CubeSat missions [17]. This experience gives us confidence in the design principles we have carried onto its PocketQube-sized counterpart.

The electronic design of PyCubed-Mini utilizes a modified form of the careful commercial-off-the-shelf (COTS) technique outlined by Sinclair and Dyer (2013) [42]. As the original PyCubed paper describes, "the intent of careful COTS is to provide an alternative to historically rigorous radiation-hardened satellite design that better fits the needs of modern small satellite projects."

Space is an extreme, high-radiation environment. The effects of consistently high radiation absorption in electronics appear as a parametric degradation that leads to functional failure. Such prolonged radiation exposure is quantified by the total ionizing dose (TID), typically represented in units of rads. On the other hand, a single-event upset (SEU) is a change of state caused by a single ionizing particle striking a sensitive node in a live electronic device, such as a microprocessor, semiconductor memory, or transistors.

Favorably, low-Earth-orbit (LEO) missions fly under the high-radiation Van Allen belts surrounding the Earth. The relatively lower radiation exposure improves the likelihood of COTS components surviving through the mission. We have established a conservative total ionizing dose (TID) threshold of 10 krad/year for our mission based on PyCubed's findings. This value is about 1-2 orders of magnitude lower than TIDs in medium-Earth-orbits (MEO) or high-Earth-orbits (HEO) within the same exposure period (Figure 2.21) [48].

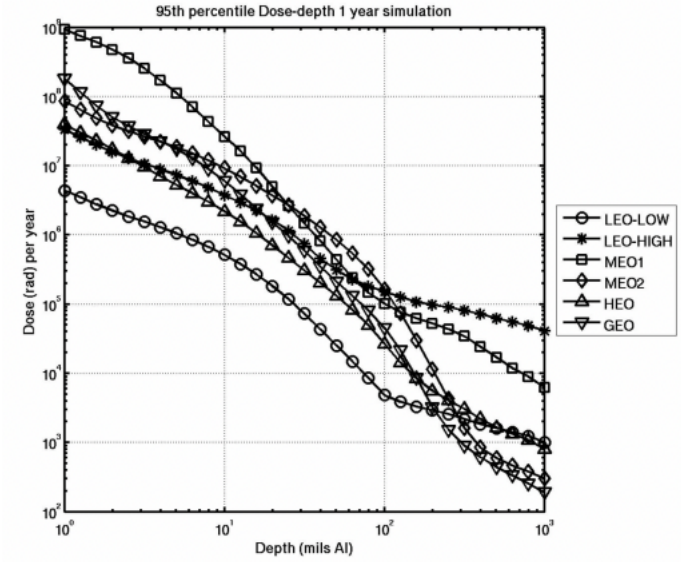

Figure 2.21: TID / year in various Earth orbits 2.21

We follow PyCubed's methodology of thoroughly understanding the radiation environment, data-driven component selection, and supplemental radiation testing [18]. We have adopted many of the components used on the PyCubed board for PyCubed-Mini. Additionally, we relied on components recommended and supported by the hobbyist electronics brand Adafruit Industries. Adafruit is the developer of the CircuitPython platform and maintains drivers for the wide selection of component breakout boards it sells. We accelerate component integration and software development by selecting from this range of components.

The global chip shortage caused by the COVID-19 pandemic [53] created a significant challenge for sourcing components during the project's early days. Components that were out of stock, prohibitively expensive, or had become obsolete since the design of the PyCubed board, were replaced and the corresponding circuitry reworked.

PyCubed-Mini's boards are designed for 50-ohm controlled impedance using the FR408HR laminate multi-layer stack-up with generous via diameters and trace widths. This stack-up reduces electromagnetic interference (EMI), emission, and absorption while maintaining signal integrity and thermal robustness. The result is a cost-effective board design that reduces manufacturing risk by not pushing the limits of modern PCB fabrication techniques and can selectively be made using more expensive laminate materials when necessary.

2.3.2 Mainboard Design

As the name suggests, the PyCubed-Mini mainboard is a miniaturized version of its namesake CubeSat-sized PyCubed Board. It is responsible for the command and control of the spacecraft, telecommunication, and data collection and storage. A 4-layer board design for the mainboard improves EMI and RF performance.

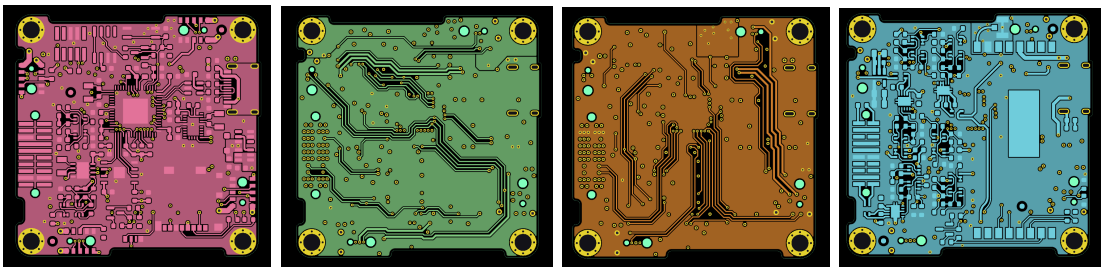

Figure 2.22: Mainboard PCB layers (top (left) to bottom (right))

Like the PyCubed board, the PyCubed-Mini mainboard uses Microchip's ATSAMD51 family of microprocessors for its high-performance ARM Cortex-M4 architecture, low power consumption, flexible pin configuration, hardware floating-point math support, on-board USB handling, and accessibility.

As the primary microcontroller unit (MCU), the ATSAMD51 is a mission-critical component. The PyCubed paper determined TID threshold limits per MIL-STD883 1019.8 for this microcontroller [18]. The processor experienced flash memory issues starting at 16 krad, whereas power and logic remained functional beyond 35 krad. The preliminary findings provided a high confidence level in the ATSAMD51's survival ability beyond our estimated mission dose levels. Furthermore, the MCU has flight heritage on several missions, including the KickSat-2 and V-R3x missions.

The mainboard has a USB-C port for flashing firmware and programming the board. USB-C connectors offer increased durability over micro-USB and mini-USB and are more compact than full-sized USB-A or USB-B connectors, making them an ideal choice. The port is accessible outside the satellite through a cut-out on the +Z solar panel board, allowing an interface for flashing and programming the mainboard even after the satellite is assembled and sealed for flight.

The specific 64-pin QFN package of the ATSAMD51 we use breaks out six serial-communication (SERCOM) ports which can be assigned to unique I2C, SPI, or UART

buses as needed [21]. On PyCubed-Mini, we have divided the SERCOM ports up as follows.

- **I2C1** (SERCOM 3), **I2C2** (SERCOM 1), **I2C3** (SERCOM4)
- **SPI** (SERCOM 2)
- **UART1** (SERCOM 0), **UART2** (SERCOM 5)

Besides these, the ATSAMD51 also possesses a Quad-SPI (QSPI) bus to enable communication between the microcontroller and its flash storage at four times the rate of a typical SPI bus.

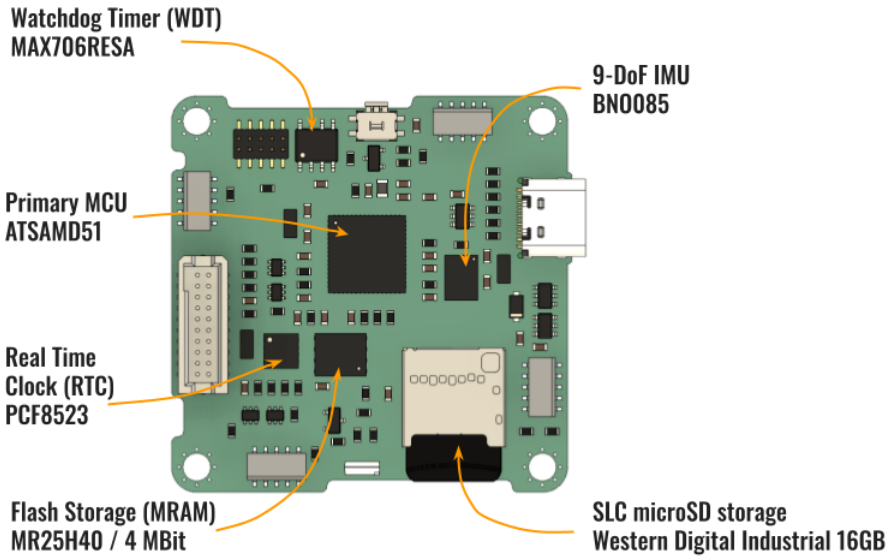

Figure 2.23: Mainboard +Y surface with components labelled

Let us explore some selected mission-critical components on board PyCubed-Mini, and the reasons for their selection:

Data-storage

The MR25H40, manufactured by Everspin Technologies, is a 4MB non-volatile magnetoresistive memory device, commonly called MRAM. Magnetoresistive memory operates in a manner inherently more tolerant to Total Ionizing Dose (TID) effects.

Cochran et al. demonstrated a TID tolerance for MRAM in the range of 90–100 krad [3], which ensures the reliable storage of critical data throughout the satellite's mission.

We have implemented a multi-gigabyte micro-SD data storage solution to accommodate large data products. In general, flash memory devices fabricated with single-level cells (SLC) tend to have higher TID thresholds compared to devices built with multi-level cells (MLC) [26]. We selected Western Digital's SDSDQED series of high-endurance SLC micro-SD cards for our missions. Any standard micro-SD card functions identically, providing the flexibility of using a low-cost component during the testing and prototyping phases.

Watchdog

Since the mainboard MCU interfaces with all major components of the satellite, it is essential to have an external watchdog timer (WDT) to reset the MCU in the case of a single-event-upset (SEU). We have chosen the MAX70X series of supervisors by Analog Devices Inc. for this purpose. Kenna et al. (2009) found a worst-case TID of 11 krad for this component [28], which is still above our conservative mission TID estimate for one year.

The MCU initiates a Pulse-Width Modulation (PWM) signal on the watchdog's input pin at boot. If the watchdog does not detect a toggle on this pin within 1.6s, it may indicate a fault on the MCU. The watchdog output goes low, triggering a hard reset of the MCU [9].

Inertial measurement unit (IMU)

A 9-DoF (Degree of Freedom) IMU integrates a 3-axis accelerometer, a 3-axis gyroscope, and a 3-axis magnetometer into one integrated circuit (IC) package.

The PyCubed board featured the popular BMX160 9-DoF IMU by Bosch Sensortec, which has since become obsolete. Thus, for the PyCubed-Mini mainboard, we elected to use the BNO085 9-DoF IMU by CEVA Technologies, Inc. This component integrates an ARM Cortex-M0 core that fuses state estimates, reducing the workload on the primary MCU. Furthermore, this component is recommended and supported by Adafruit for modern 9-DoF applications.

The BNO085 can communicate with the system host over various serial interfaces: SPI, I2C, and UART. For PyCubed-Mini, we have opted for a UART interface between this BNO085 IMU and the ATSAMD51 MCU. It is the only component on that specific UART bus, allowing for fast communication and increased reliability [43].

Real-time clock (RTC)

PyCubed-Mini enhances the capabilities of the PyCubed board by incorporating a discrete real-time clock (RTC). Drawing power directly from the batteries, the RTC remains active even if the other power buses are disabled - which may be required to recharge its batteries - or when the satellite is reset, such as in the event of an SEU. Its accurate timekeeping is crucial for our guidance, navigation, and control (GNC) system and for precise data logging.

For this purpose, we opted for the PCF8523, manufactured by NXP Semiconductors, for its ultra-low power consumption, compact size, and the added advantage of CircuitPython driver support from Adafruit, which facilitates seamless integration into our system [41].

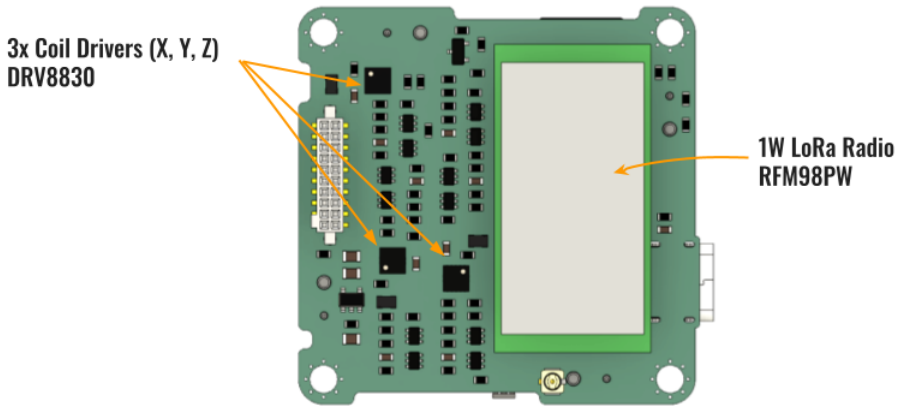

Figure 2.24: Mainboard -Y surface with components labeled

Coil drivers

PyCubed-Mini incorporates three Texas Instruments DRV8830 low-voltage motor drivers. Each motor driver powers a pair of magnetorquer coils on opposing faces of the satellite along the X, Y, and Z axes. The satellite can power each axis independently, generating a 3-axis magnetic dipole that can interact with the Earth's magnetic field and generate torque for attitude control. This approach will be discussed further in the Attitude Determination and Control System (ADCS) section.

The DRV8830 interfaces with the mainboard microcontroller through an I2C serial connection, which enables satellite attitude control through Python scripting (via CircuitPython drivers). With up to 9 configurable I2C addresses, all three motor drivers can be placed on the same I2C bus, simplifying PCB routing on the mainboard [22].

Radio

PyCubed-Mini incorporates the popular RFM98PW LoRa radio module from HopeRF. With +30dBm (or 1 watt) of transmitting power, the RFM98PW is suitable for satellite-to-ground communication. These modules have a proven track record in space, having been used on the PyCubed CubeSat motherboards.

The radio module interfaces with the ATSAMD51 microcontroller through an SPI serial connection. Radio transmission (TX) and reception (RX) can be easily controlled through simple Python scripting using supported CircuitPython drivers from Adafruit. The following section will explore the radio module's role in the broad communication system [20].

2.4 Communications System

2.4.1 Radio Module

As mentioned in a previous section, the popular RFM98PW LoRa (Long Range) radio module manufactured by HopeRF powers PyCubed-Mini's communications system. By default, PyCubed-Mini operates on the 433MHz radio frequency band but can be configured to operate on the 169MHz, 470MHz, 868MHz, or 915MHz bands as well. The RFM98PW is a fully contained module possessing circuitry for both RX and TX and can be powered directly from PyCubed-Mini's batteries to meet its power demands. The radio module also features an inbuilt temperature and low-battery sensor.

In the 433MHz and 470MHz configurations, the satellite has a maximum TX power of +30dBm (1W) and a maximum RX power of +10dBm (10mW). Equation 2.1 represents a conversion of power between units of milliwatts (mW) and units of decibel-milliwatts (dBm). The RFM98PW uses the LoRa modulation protocol by default but can also use the FSK, GFSK, MSK, GMSK, or OOK modulations [20].

$$P_{\text{dBm}} = 10 \cdot \log_{10}(P_{\text{mW}}) \tag{2.1}$$

LoRa, short for Long Range, is a low-power, long-range wireless communication technology designed for Internet of Things (IoT) and Machine-to-Machine (M2M) applications. Developed by Semtech, LoRa enables efficient transmission of small data packets over long distances, making it ideal for connecting remote and battery-operated devices. It operates in the license-free industrial, scientific, and medical (ISM) radio bands, providing excellent penetration through buildings and urban environments. LoRa employs a spread-spectrum modulation technique to achieve its exceptional range while consuming minimal power, prolonging the battery life of connected devices. The technology offers a cost-effective and reliable solution for applications such as smart cities, agriculture, asset tracking, environmental monitoring, and even space communications [6].

The mainboard microcontroller controls the radio module through a hardware SPI

interface. Adafruit has developed drivers that allow easy control of the RFM98PW modules using simple Python programming via CircuitPython.

The RFM98PW module attaches to the -Y side of the mainboard. A metal shield caps the module with a metal shield to minimize electromagnetic interference (EMI) on surrounding components. This shield effectively acts as a Faraday cage, containing stray electromagnetic noise. The RF signal is routed from the module to the satellite antenna on the -Z solar panel through a thin coaxial cable designed for a 50-ohm impedance. Cutouts in the edges of the mainboard and bottom-battery board provide the necessary space for routing this cable through the satellite, ensuring there is no mechanical interference that may lead to kinking or pinching of the cable. All traces on the RF line are also sized and routed to maintain a 50-ohm impedance.

Designing PCBs for RF applications demands careful consideration of specific factors to ensure optimal performance and minimal signal degradation. RF signals are highly sensitive to impedance mismatches, signal losses, and noise interference. Therefore, maintaining controlled impedance throughout transmission lines is crucial to minimize signal reflections and maintain signal integrity. Grounding and decoupling techniques become critical to reduce unwanted coupling and noise. Additionally, avoiding signal traces crossing gaps or splits in ground planes helps prevent disruptions in RF signal paths. Proper RF substrate materials, such as high-frequency laminates, ensure low dielectric losses and improved signal propagation [37].

The satellite's small physical size and the short RF line routing further reduce the risk of signal degradation.

2.4.2 Antenna Design

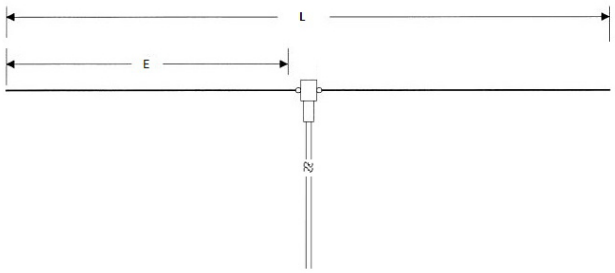

Figure 2.25: Simplified half-wave dipole antenna. *credit: everything RF*

PyCubed-Mini features a typical half-wave dipole antenna configuration. In keeping with the use of low-cost and accessible components, PyCubed-Mini's antennas are crafted from "narrow" (1/4 inch) measurement tape. The choice of measuring tape antennas is advantageous due to their springiness, allowing them to return to an extended state when deployed.

The length of a dipole (L) affects its resonant frequency (f). As the name suggests, the dipole length for a half-wave antenna should equal half the resonant frequency's wavelength. For operation on the 433 MHz frequency band, the dipole length can be determined using equation 2.2, where A is the end effect factor, approximately 0.95:

$$\begin{aligned} L &= \frac{\lambda}{2} \cdot A \\ &= \frac{c}{2f} \cdot A \\ &= \frac{3 \times 10^8}{2 \cdot 433 \times 10^6} \cdot 0.95 \\ &= 0.33 \text{ m} = 33 \text{ cm} \end{aligned} \tag{2.2}$$

Thus each antenna pole should be $E = L/2$ or 16.5 cm long.

The angle between the two poles determines the dipole's impedance. For the desired 50 ohm impedance, the angle is approximately 90 degrees. On PyCubed-Mini, we fix 3D-printed structures under the antennas during calibration that wedge them at the required angles (Figure 2.26).

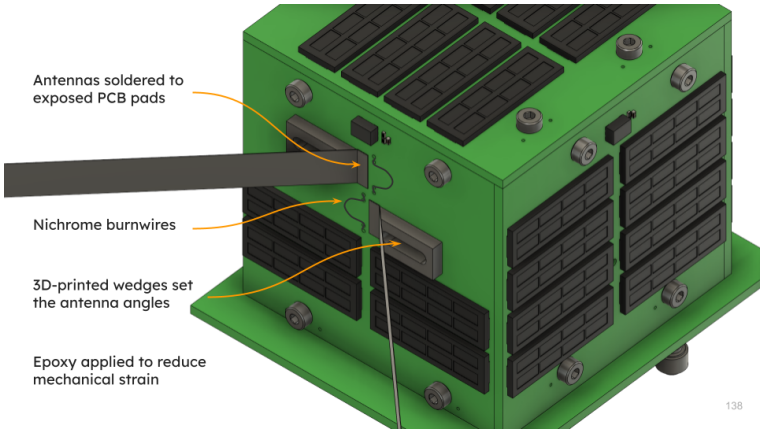

Figure 2.26: PyCubed-Mini dipole antenna mounting

2.4.3 Antenna Mounting and Deployment

Soldering the antennas to mounting pads on the -Z solar panel connects them to the satellite's RF (Radio Frequency) circuit. These pads must be designed as small as possible. Larger pads act as miniature antennas, wasting transmission power on arbitrary frequencies and degrading overall communication quality.

Smaller attachment points held solely by solder are mechanically in-stable and may result in antenna separation during deployment. In order to prevent such a catastrophic failure, the antenna mounting point is staked with epoxy, limiting the mechanical strain on the joint while stowed and preserving the dipole angle when deployed.

The unbalanced coaxial signal passes to a balun on the -Z solar panel. A balun (from "balanced to unbalanced") is an electrical device that allows interfacing balanced and unbalanced lines without disturbing the impedance arrangement of either line. Thus, a balanced dipole signal of 50-ohm impedance is produced and routed to each dipole antenna. Once again, we take great care in the RF circuit's design, component placement, and routing on the antenna board.

The -Z solar panel board is equipped with a burn-wire circuit (Figure 2.27) responsible for powering two separate burn-wires in series, one for each antenna (Figure 2.26). Since the successful deployment of the antennas is critical for the mission's success, we use radiation-tolerant components to assemble the burn-wire circuit.

The ends of each antenna are hole-punched, and a thin fishing line is threaded through each hole. The antennas wrap around the satellite, and the fishing line is tied to the burn wires, keeping the antennas stowed under tension.

Nichrome wire is commonly used as a heating element because of its high melting point and low oxidation rate. During deployment, the burn-wire scheme completes the circuit between the batteries (BATT_P) and ground through the burn-wires. This scheme effectively creates a short circuit across the battery. A large current subsequently passes through the burn wires, heating them and causing the fishing line to melt and detach. This results in the antennas unfurling into the required dipole shape (Figure 2.28).

Most battery packs will activate their short-circuit protection if the current is

drawn this quickly. In the case of the PyCubed-Mini software, we turn the burn-wire circuit on and off very quickly through pulse width modulation (PWM) (BURN1 line) to regulate the current below the short-circuit threshold. A tuned resistor in series with the burn wires (R34) further limits the peak power drawn from the batteries.

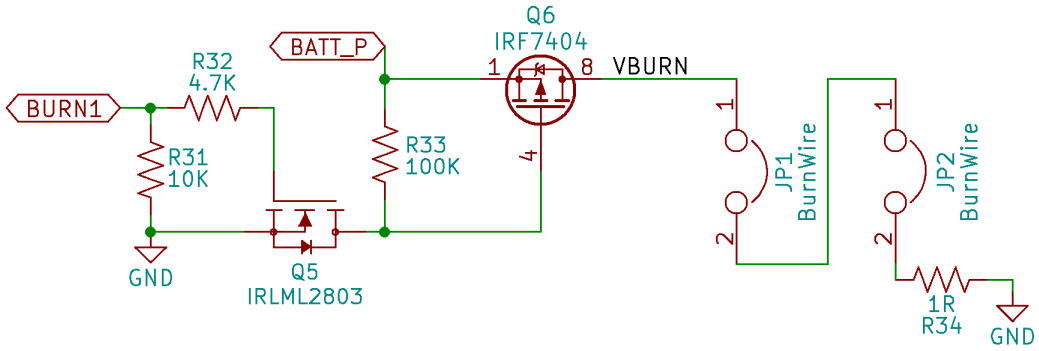

Figure 2.27: Burn-wire circuit

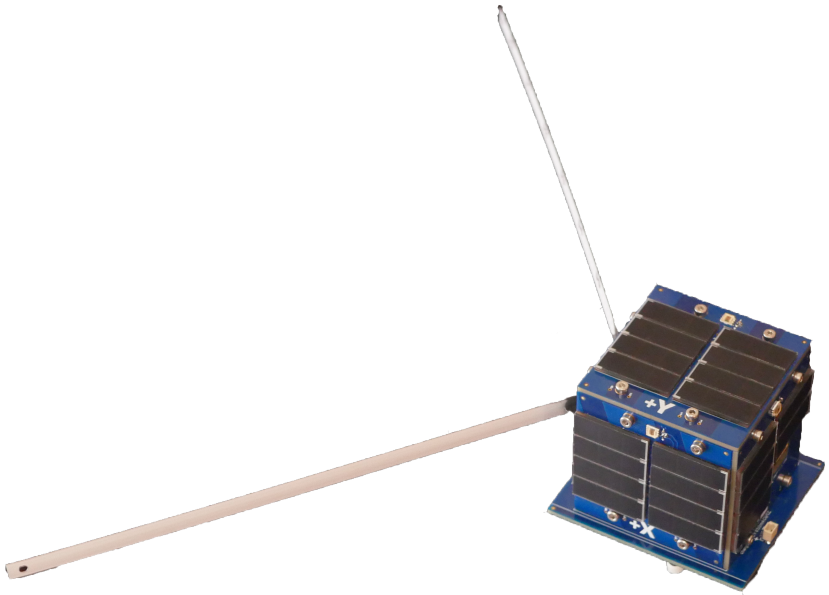

Figure 2.28: PyCubed-Mini with its antennas deployed

2.5 Attitude Determination and Control System (ADCS)

2.5.1 Attitude Determination

An OPT4001 I2C high-precision digital ambient light sensor (ALS) is installed on each face of the satellite. These devices feature 28 bits of effective dynamic range from 437.5 µlux to 117 klux of light intensity, which makes them suitable for measuring the intensity of sunlight [25]. By processing the illumination levels on the six light sensors, we can calculate the vector of the sun relative to the satellite.

The sun vector estimate, combined with accelerometer and gyroscope data from the mainboard IMU, is processed through a Kalman filter on the primary MCU to estimate the satellite's orientation in space.

2.5.2 Attitude Control

Typical attitude control methods, such as reaction wheels and reaction control system (RCS) thrusters, are too large, complex, and expensive to be feasible on the scale of a PocketQube satellite. Instead, PyCubed-Mini features a magnetorquer-only attitude control system.

A magnetorquer is a satellite system for attitude control, de-tumbling, and stabilization built from electromagnetic coils. Magnetorquers are lightweight, reliable, and efficient. Unlike thrusters, magnetorquers do not rely on expendable propellant and can function indefinitely as long as sufficient power is available. A notable advantage over momentum wheels and control moment gyroscopes is their lack of moving parts, greatly enhancing reliability.

The magnetic dipole generated by magnetorquers (μ) can be controlled by switching current flow on or off through the coils on the X, Y, and Z axes under computerized feedback control. The resultant magnetic dipole interacts with Earth's ambient magnetic field (B), so the produced counter-forces provide useful torque, making it possible to freely pivot the craft around in a known local magnetic field gradient by only using electrical energy.

The control torque τ is governed by equation 2.3 and illustrated in Figure 2.29.

$$\tau = \mu \times B \tag{2.3}$$

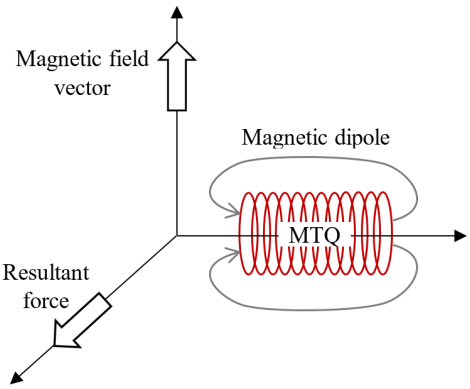

Figure 2.29: Magnetorquer operating principle illustrated [31]

The cross product in the above equation, nonlinear attitude dynamics, and the time-varying magnetic field along an orbit make this an underactuated, nonlinear, time-varying control problem. To solve it, we use iterative LQR. Gatherer and Manchester (2019) [14] discuss the specific methodology for solving this problem, the details of which are beyond the scope of this thesis.

2.5.3 Magnetorquer Design

Typical CubeSat designs with integrated magnetorquer coils feature discrete modules composed of tightly wound copper wire over a non-conductive core anchored to the satellite. Larger satellites may feature torque rods wherein a current through a conductive wire wrapped around a ferromagnetic core magnetizes it, generating a considerably higher dipole.

Due to the small physical size and mass limit of a PocketQube satellite, the above magnetorquer implementations are infeasible. PyCubed-Mini utilizes an embedded coil design that implements magnetorquers by routing spiral traces on the internal layers of the satellite's solar panel PCBs (Figure 2.30). This implementation requires

no extra volume as the existing structure of the satellite entirely contains the coils. However, the magnetic dipole magnitude is much lower due to the limited number of coils and the presence of other circuits.

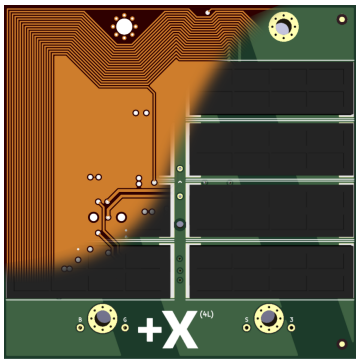

Figure 2.30: Solar panel PCB inner layers with integrated magnetorquer coils

We, however, benefit from the fact that the control authority of magnetorquers gets larger as the satellites they control get smaller.

On PyCubed-Mini, the magnetorquer coils are driven by three DRV8830 H-bridge motor drivers installed on the mainboard - one for each axis. Each motor driver powers a pair of magnetorquer coils on opposing faces of the satellite along the X, Y, and Z axes. The satellite can thus power each axis independently. The coils on an axis are connected in series such that the current flow is clockwise on the positive (+) axis board and counter-clockwise (-) on the negative axis board. Thus, considering the right-hand rule, the resultant magnetic dipole is directed towards the positive axes.

The solar panels are 4-layer PCBs by default, with the two internal layers, each routed with 19 trace coils. The PCB design can easily extend to 6 or more layers, multiplying the number of magnetorquer coils. More coils have the advantage of lowering the current demand from the coil driver ICs, with the disadvantage of an increase in manufacturing cost and turn-around times. Given the number of coils, N, the current through them, I, and their area of cross-section, A, the magnitude of the dipole moment, $\vec{\mu}$ may be calculated as:

$$\vec{\mu} = NIA \tag{2.4}$$

In a 6-layer PCB, four layers have coils routed on them, which doubles the number of coils relative to a 4-layer PCB. However, since the resistance of a conductor is proportional to its length, the coils of 6-layer PCBs have twice the resistance of the coils of the 4-layer PCBs. Since $I = V/R$, and the driving voltage of the motor drivers is unchanged, the magnitude of the electric current is halved. The average cross-sectional area of coils remains unchanged. Thus, from equation 2.4, we can determine that increasing the number of PCB coil layers has no impact on the magnitude of the dipole moment.

2.6 Payload / Vision System

2.6.1 Camera Module

While PyCubed-Mini's design is remarkable for its simplicity and ease of use, it has no shortage of powerful and innovative features. Below the mainboard in the avionics stack is integrated the cameraboard, configured with a 5-megapixel (2592x1944) camera module.

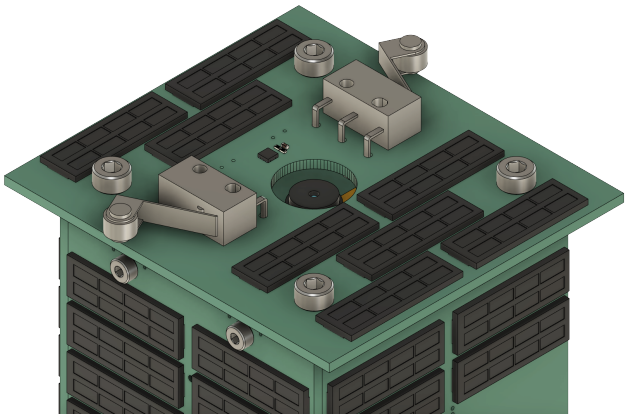

Figure 2.31: Camera module viewed through porthole cut-out on -Y solar panel

The camera module incorporates the popular OmniVision's OV5640 5MP camera sensor, coupled with a 2.8mm focal length lens with a fixed aperture of F2.8 and a diagonal field-of-view (FOV) of 63 degrees. It is mounted to the bottom of the cameraboard and looks out into space through a cut-out in the -Y solar panel board (Figure 2.31).

The camera module electrically connects to the cameraboard through a ribbon cable and latched 24-pin flat-flex connector (FFC). It can thus be easily swapped out with alternatives possessing different optical parameters, resolutions, or spectral ranges, tailoring the cameraboard to the mission's needs.

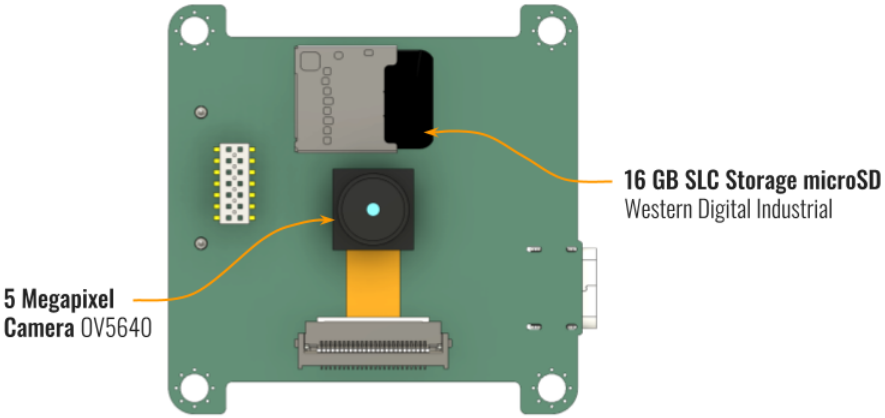

Figure 2.32: Components on the -Y surface of the cameraboard

2.6.2 High Performance Microcontroller

The cameraboard has a high-performance STM32H7 microprocessor running at 480MHz, enabling rapid, high-resolution imaging. The STM32 operates the camera through an I2C-compatible Serial Camera Control Bus (SCCB) and communicates data via an 8-bit parallel Digital Video Port (DVP).

The Open Source Satellite (OSSAT) project, in collaboration with the Surrey Space Centre at the University of Surrey, UK, evaluated the STM32H7 microprocessor to assess its resilience in the challenging space radiation environment. The results indicated that the internal flash memory exhibited signs of failure at a 47 krad Total Ionizing Dose (TID) [1]. This radiation tolerance level surpasses our anticipated mission dose of 10 krad, providing us with great confidence in the durability and survivability of our cameraboard design.

We aim to leverage the capabilities of the cameraboard MCU to execute advanced computer vision algorithms onboard our satellite.

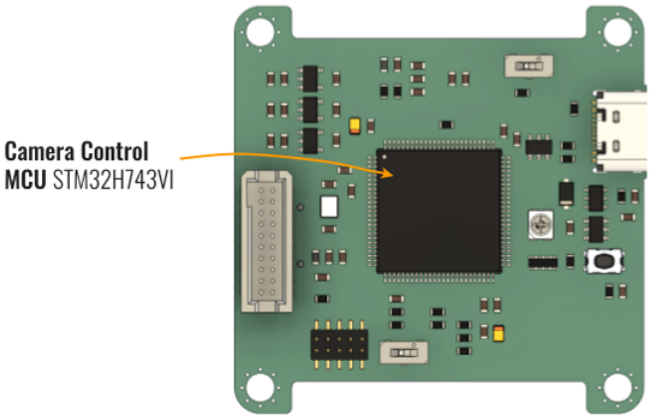

Figure 2.33: Components on the +Y surface of the cameraboard

2.6.3 Software and Peripherals

We have based the cameraboard hardware and firmware design on the popular, open-source OpenMV camera modules (www.openmv.io). Leveraging OpenMV's MicroPython-based firmware, we enable programming in Python and benefit from their extensive collection of in-built machine learning and image processing algorithms. OpenMV's mission to make machine vision more accessible to beginners aligns perfectly with our objectives.

The cameraboard is equipped with its own industrial Western Digital SDSDQED SLC micro-SD card for local storage of images or data products prior to processing and transmission. This card proves advantageous during development, allowing developers to access data or debug logs easily by plugging it into an external computer.

Like the mainboard, the cameraboard possesses an externally accessible USB-C port to flash the firmware on and program the microcontroller. It also has its implementation of the high-power selection circuitry, which allows the board to be preferentially run off of USB power when it is available.

2.6.4 Cameraboard / Mainboard Interface

The cameraboard interfaces with the mainboard over a high-speed UART bus. This arrangement allows the mainboard to retain complete control of the cameraboard

while offloading all the CV computations to the more powerful microcontroller. The mainboard receives the results of the CV processing, which can be further processed, stored, or transmitted. Additionally, the mainboard can request raw images from the cameraboard. However, due to the mainboard's limited memory reserves, only single images may be sent, which must be packetized on the cameraboard before transmission.

One drawback of powerful hardware is high power consumption and heat production. Three linear voltage regulators step down the battery voltage to the levels required by the microcontroller and camera module. The mainboard MCU can toggle the voltage regulators and thus turn the cameraboard on or off. In order to limit the power consumption and heat production by the cameraboard, the mainboard turns it on only when needed.

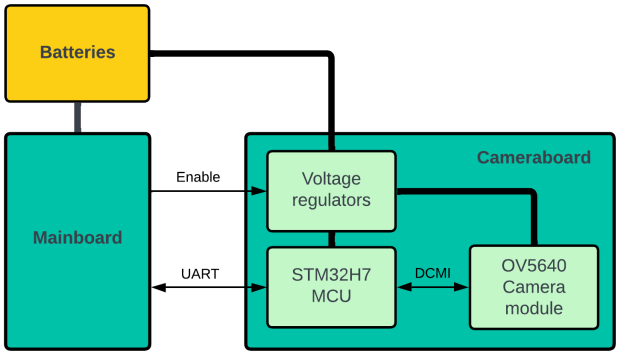

Figure 2.34: Cameraboard / Mainboard Power and Data Interface

Careful circuit board design can significantly improve heat dissipation. Large ground planes and thermal stitching vias under and around heat-producing components rapidly wick away heat and prevent overheating. We omit the solder mask under the camera module and mount it directly to bare copper using epoxy with high thermal conductivity.

If a camera is deemed unnecessary for a particular mission, the cameraboard can be easily redesigned with any other custom payload to suit specific requirements. This payload flexibility opens up possibilities for incorporating diverse modules, such as specialized communications, GPS modules, FPGAs, or for space verification of custom silicon.

2.7 Novel Bus Protection Circuitry

Serial communication buses are used in electronics to link sensors and other devices. However, the most extensively utilized protocols, I2C and SPI, are susceptible to system-wide breakdowns if just one device on the bus encounters a malfunction. The compounding risk to overall system reliability as the number of devices on a bus increases becomes a restricting element for aerospace applications that require distributed processing and sensing capabilities — posing limitations on mission scope, performance, and lifespan.

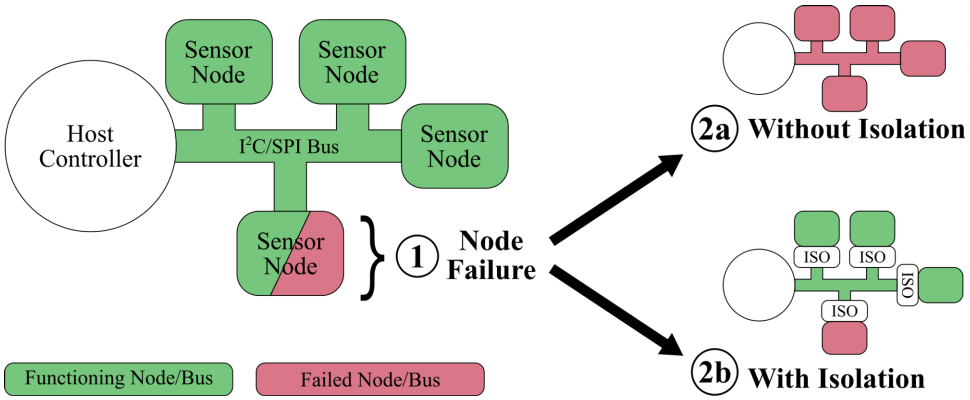

Figure 2.35: Impact of a single failed node on its serial bus - with and without isolation schemes [19]

The impact that the number of devices (n) on a bus has on system reliability can be modeled as a series system. Assuming all devices have the same probability of failure (P):

$$P(\text{system failure}) = 1 - (1 - P)^n \tag{2.5}$$

That means the probability of bus failure increases exponentially with device count, necessitating the need to implement discrete isolation schemes for devices on such serial buses. Holliday et al. [19] devised automatic isolation circuits for I2C and SPI communication buses to prevent bus-wide failure in the event of a single device malfunction without requiring additional I/O or processing overhead. We have

implemented these schemes on each I2C or SPI device within our satellite system.

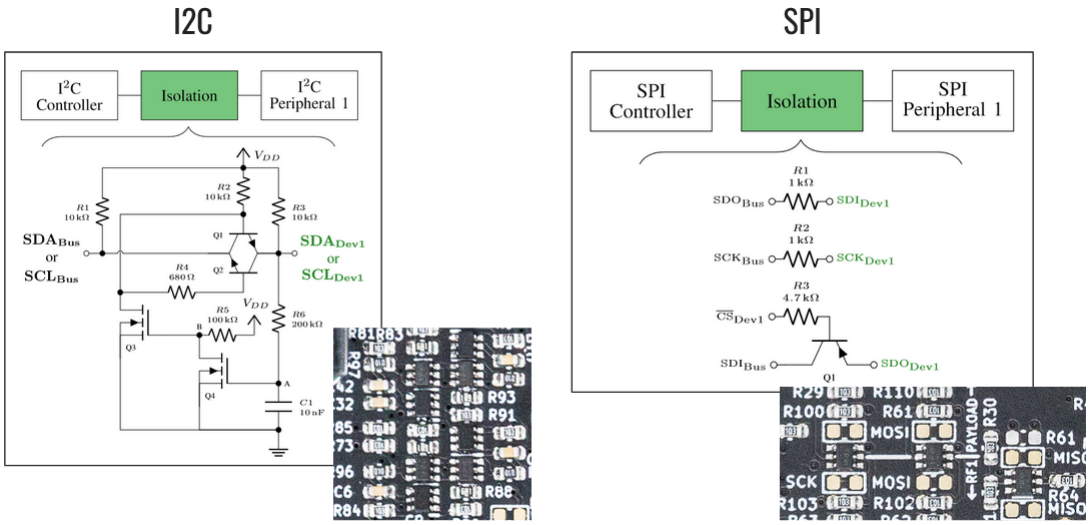

Figure 2.36: Schematic and layout of discrete isolation schemes: I2C (left) and SPI (right) [19]

Chapter 3

Manufacture, Assembly, and Testing

This chapter will discuss our considerations in manufacturing our satellite hardware, the choices to optimize the assembly process, and the procedures adopted for performing comprehensive testing to verify and validate the functionality of a newly assembled PocketQube satellite.

3.1 Manufacturing and Procurement

3.1.1 Outgassing Considerations

PLA 3D-printing filament, known for its ease-of-use and low-cost, is a popular choice for prototyping mechanical structures. However, PLA's high outgassing nature means that flight components must undergo a comprehensive bake-out process before launch. Additionally, PLA's low melting point and poor mechanical characteristics make it unsuitable for space applications.

To address these limitations of standard 3D-printing filaments, we have used Windform XT 2.0, a carbon-fiber-reinforced composite material manufactured by CRP Technology, for our flight mechanical structures. This material offers improved mechanical strength and thermal stability and complies with NASA and ESA's outgassing requirements [44] [45].

This composite has space heritage on several CubeSat missions [47] and is also the material used by Alba Orbital to build their PocketQube deployment pods, AlbaPod V2, which have deployed several PocketQube missions (Figure 3.1) [46].

Figure 3.1: AlbaPod V2 PocketQube deployment pods, constructed out of Windform XT 2.0 composite. *credit: Alba Orbital*

3.1.2 PCB Manufacture

The cost of printed circuit board fabrication has declined significantly with time, which has energized the hobbyist electronics design community. PCB manufacturers in China, especially, offer rock-bottom fabrication prices for high-quality circuit boards with good tolerances. Many of these board houses also offer PCB assembly services for a small up-charge. There are still several considerations when ordering PCBs for space systems, as these can significantly affect prices.

IPC (Institute for Printed Circuits) has established quality standards that govern the manufacturing and assembly of printed circuit boards. These standards define the requirements for the reliability and performance of electronic components.

IPC Class 3 standards have the most stringent requirements, such as tight tolerances for trace widths and spacing, controlled impedance, and specific material selections, to ensure greater robustness in harsh environments, where safety, longevity,

and precision are critical. IPC Class 3 assemblies undergo more rigorous testing and inspection procedures as well.

Consequently, PCBs manufactured to IPC Class 3 standards can cost thousands of dollars, making them unsuitable to meet our project goals. Thus, we have designed our boards to maintain high reliability even within the weaker tolerances of the more common, low-cost IPC Class 2 manufacturing standard. By using generous trace sizes, spacing, and sufficiently large vias, we avoid approaching the limits of modern PCB manufacturing.

Interconnect Failure

Interconnect failure is a common environmentally induced failure mode for PCBs that manifests as solder joint fractures and plated-through hole (PTH) separation resulting from thermal or vibration-induced fatigue (Figure 3.2). Thermal-mechanical fatigue can be significantly reduced by selecting a PCB laminate material with a lower coefficient of thermal expansion (CTE) compared to traditional FR4 laminates [18].

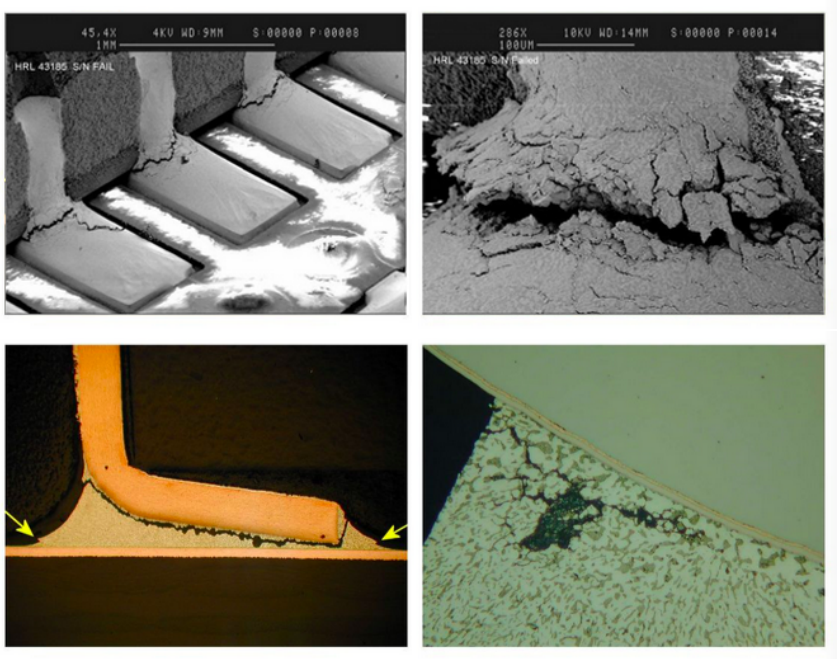

Figure 3.2: Interconnect failure [7]

CTE is typically associated with the laminate's glass-transition temperature (Tg) - the temperature at which an amorphous polymer changes from a hard/glassy state to a soft/leathery state and is about 130-140 degrees Celsius for FR4. A laminate with high Tg and low CTE can reduce thermal-mechanical fatigue. For example, the FR408HR laminate material made by Isola Group is a widely available PCB material that reports a Tg of 190 degrees Celsius and a 30% improvement in Z-axis expansion [15].

Board House Selection

We have explored several low-cost board houses for manufacturing the PCBs on our satellite. Table 3.1 represents the results of this trade study. Since the PCBs form the bulk of our satellite, the cost of fabrication drives the overall cost of the satellite.

	2 layer board	Turnaround time	4 layer board	Turnaround time
China Board houses				
JLCPCB	Tg 130: $3.5 / board	3-4 days	Tg 155: $14 / board	3-4 days
PCBWay	Tg 175: $17 / board Tg 155: $8.50 / board	3-4 days	Tg 175: $31 / board Tg 155: $15 / board	4-5 days
USA Board houses				
OSHPark	Tg 175: $5 /board	9-12 days	Tg 175: $11 / board	9-14 days
DKRed	Tg 175: $5 /board	10 days	Tg 175: $10 / board	10 days

	6 layer board	Turnaround time	Shipping cost	Notes
China Board houses				
JLCPCB	Tg 155: $11 / board	5-6 days	~$20	5 board minimum
PCBWay	Tg 175: $72 / board Tg 155: $35 / board	10-11 days	~$20	5 board minimum
USA Board houses				
OSHPark	Tg 175: $19 / board	9-14 days	Free	3 board minimum
DKRed	N/A	N/A	< $10	4 board minimum

Table 3.1: Board house trade study. 1.6 mm PCBs with 1 oz/ft^2 copper deposition, default solder mask color, and ENIG surface finish. Prices representing highest Tg substrates

While board houses from China offer highly competitive pricing, their boards typically exhibit weaker tolerances and are relatively lower quality. For example, we found that such boards are more prone to having thin pads rip off the substrate if assemblers are rough-handed with their soldering. Nevertheless, we have yet to encounter any issues with circuit functionality from these boards thus far.

Fabrication costs in the US increase dramatically with increasing board sizes. However, we have found that for our small PCBs, the cost difference is minor, with some US-made PCB configurations being cheaper than their Chinese equivalents at this scale. US board houses usually have longer turnaround times - however, when factoring in the time required for shipping boards from China, delivery times are also similar. US-manufactured boards usually have better tolerances and, by default, will use high-quality substrates necessary to avoid interconnect failure - as discussed in the previous section.

The board houses we have studied each have their pros and cons:

- **JLCPCB**: Extremely low prices, but only offer 155 Tg or 130 Tg (for 2-layer boards) substrates. The boards are somewhat lower quality than the rest. However, we use them regularly for board prototypes and their low-cost 6-layer boards. They also offer 8+ layer PCBs for reasonable prices.
- **PCBWay**: Offer high Tg substrates and relatively higher quality boards than JLCPCB. Prices are typically a lot higher for multi-layer boards.
- **OSHPark**: High-quality boards manufactured with high Tg substrates and ENIG surface finishes by default. Relatively longer turnaround times. They manufacture 6-layer boards for reasonable prices. OSHPark does not remove panel tabs from their PCBs, so boards require some post-processing.
- **DKRed**: Similar quality to OSHPark. Offer a fast turnaround option which makes them a good choice for flight boards. Do not manufacture 6+ layer PCBs and do not support slots within PCBs, making them unsuitable for boards like the +Z or -Y solar panels.

3.1.3 Automotive-Grade Component Selection

While military-spec or space-grade parts are ideal for the extreme environmental conditions of space, they are typically prohibitively expensive, ITAR regulated, or have impractically long lead times. In keeping with our careful COTS design methodology, a simple consideration to improve satellite reliability is selecting automotive-grade components versions when available. Such components are typically rated for a wider temperature range and have undergone more stringent stress and failure tests in compliance with test qualifications set out by the Automotive Electronics Council (AEC).

Most passive components and many ICs have pin-compatible automotive-grade versions. Usually, the cost premium of these components is insignificant compared to the performance benefits they provide. For our PyCubed-Mini builds (both prototype and flight models), we opt for the automotive-grade version of a component whenever it is available.

3.2 Assembly Practices

3.2.1 Optimizing Design for Assembly

As described in the structural design section, PyCubed-Mini features no precision-manufactured components. Its mechanical structures can be prototyped in under 40 minutes on conventional 3D printers using commonly available filaments. The solar panels are attached using basic COTS hardware, such as M2 and M3 metric screws, to threaded heat inserts incorporated within the 3D-printed structures. These inserts can be quickly and securely installed using a basic soldering iron.

PyCubed-Mini's circuit boards can be fully hand-assembled using a soldering iron, hot air gun, good quality solder, flux, and a small amount of patience. We have taken care to use a minimum 0603 package size (0.06" $\times$ 0.03") for all passives (resistors, capacitors, and inductors). This package size strikes a good balance between being comfortable to solder and not occupying much physical space on the boards.

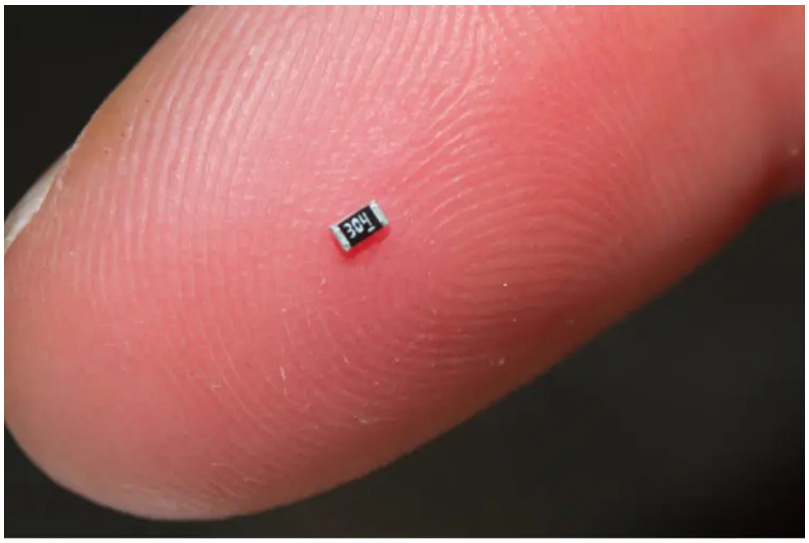

Figure 3.3: The size of an SMD resistor in a 0603 package, relative to a human finger [credit: Ultra Librarian]

For integrated circuits (ICs) and other active components (such as transistors or diodes), we have preferred legged packages, if available, provided we can accommodate their relatively larger footprints. Reliability issues with soldering quad flat no-lead (QFN) packages have been well documented [29], and legged packages have the additional advantage of being easier to solder.

Once all the mechanical components and circuit boards have been individually assembled, they can be integrated into the complete satellite assembly in about 5 to 10 minutes, using nothing more than a screwdriver kit.

3.2.2 Optimizing Assembly for Design

Often Flat no-leads IC packages (like QFN) must be utilized due to a lack of legged alternatives or physical space on the boards. These components can be challenging to hand-solder for individuals with limited experience. Prolonged or repeated heating - as may occur due to poor soldering technique - may damage components and affect the reliability of the satellite system.

Due to the large number of components on some boards, hand assembly may take several hours. Reflow soldering may help speed up assembly. It can also make soldering QFN packages easier. Following the recommended reflow profile for the

solder paste reduces the risk of thermal damage. The drawback of this approach is an increased likelihood of poor connections, solder bridging, or the formation of tiny solder balls, which may be difficult to detect but result in electric shorts.

Furthermore, reflowing PCBs with components on both sides is challenging since the solder joints melt simultaneously, causing the components on the bottom to detach. A way to circumvent this issue is to use regular "high-temperature" solder to reflow the first side and special low-temperature solder for the other side. The low-temperature solder melts first, while the joints on the bottom stay solid due to their higher melting point.

As mentioned previously, many PCB manufacturers offer low-cost PCB component assembly. These board houses typically stock commonly used components and will purchase any unavailable components from retailers like DigiKey and Mouser as requested by the customer. This avenue is ideal for teams with insufficient soldering experience. We must, however, consider the IPC Class 3 standard for PCB assembly. Careful hand-soldering can meet IPC Class 3 standards; however, board assembly houses usually charge a significant premium for IPC Class 3 assembly.

3.2.3 Solder Selection

The aforementioned 2-side reflow technique is acceptable for prototype boards; however, low-temperature solder should be avoided for the flight build, as these are usually lead-free solders, which are not advisable for aerospace projects [4].

Lead-free solder is more likely to fracture in high shock and vibration environments. A unique property of Lead-free solders with high Tin content is the possibility of their joints spontaneously growing so-called "Tin-whiskers" (Figure 3.4). These thin filaments of Tin can grow up to 20 mm in length and cause electrical shorts between components and subsequent malfunctions. Failures on spacecraft relating to the growth of metal whiskers have been well-documented [38].

Figure 3.4: Tin whiskers

The exception to exclusively using leaded solder is that PyCubed-Mini's solar cells must be soldered using low-temperature solder, as recommended by their datasheet. At the high temperatures required for leaded solder, the solder cells may delaminate and melt, permanently damaging them in the process.

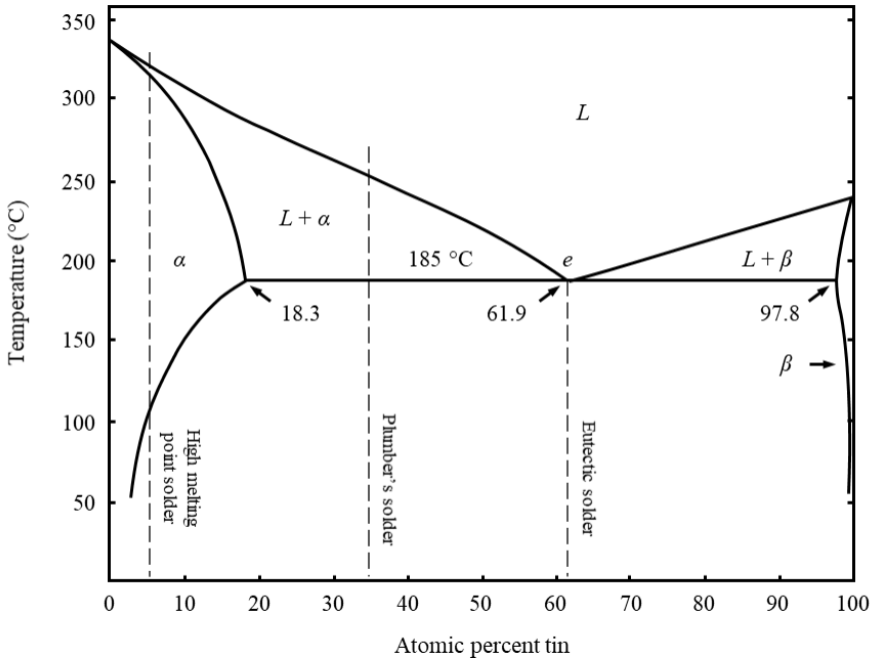

Figure 3.5: The lead-tin (Pb-Sn) phase diagram with three different solder compositions marked out; one eutectic, and two non-eutectic (Plumber's solder and a high melting point solder) [32]

Several leaded solders exist with varying ratios of composition. We opted for the popular 63% Tin (Sn) and 37% Lead (Pb) solder. This particular composition has the advantage of being eutectic. Eutectic solders are alloys that melt and solidify at one single temperature (Figure 3.5). In non-eutectic solders such as the popular 60/40 Lead/Tin mix, one component melts before the other, resulting in the two slowly separating from each other within the alloy mix - which can result in weak solder joints, making non-eutectic solder unsuitable for high shock and vibration environments.

3.2.4 Antenna Board Assembly

We use a Dremel polishing tool to remove the paint from one end of the tape measure antennas, exposing the bare metal for soldering. Coarse sanding of the smooth metal surface removes oxidation and ensures better solder adhesion. Soldering the antennas onto the -Z solar panel board's antenna pads connects them to the RF circuit.

Other parts of the RF circuit may affect our calculated antenna parameters. We use a Vector Network Analyzer (VNA) to determine the antenna's actual resonant frequency and impedance. The dipole antennas are initially oversized and then progressively trimmed in equal amounts until they exhibit the desired resonant frequency. Using measuring tape for the dipole also has the advantage of having printed length markers, enabling precise trimming.

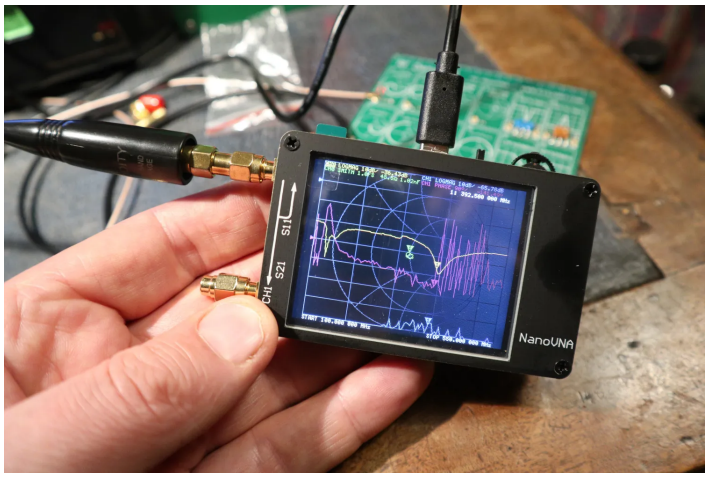

Figure 3.6: A Nano-VNA (Vector Network Analyzer). A $60 device that can measure antenna parameters such as resonant frequency and impedance.

To maintain the tuned angle for a 50-ohm dipole impedance, we designed 3D-printed mechanical braces that fit under the antennas and wedge them at the calibrated angle. The antenna solder joints are staked with epoxy to reduce mechanical strain during deployment.

The Nichrome wire used for the burn wires gets very hot during a burn. Hand oils or other contaminants can react with the Nichrome, causing pitting, cracks, and eventually failure. Care must also be taken not to kink the wire or bend sharply in the exposed loop.

3.2.5 Microcontroller Programming

New microcontroller chips are shipped blank and must be flashed with a bootloader after being soldered. For the ATSAMD51 mainboard MCU, we use Microsoft's uf2-samdx1 bootloader. This USB Mass Storage bootloader mounts the board as a USB drive, allowing firmware and software programming by simply dragging and dropping the files into the mounted folder. The bootloader image is flashed from the Microchip Studio PC application via a Serial Wire Debug (SWD) port on the mainboard. We use Segger's popular J-Link debug probes to interface the computer and the mainboard.

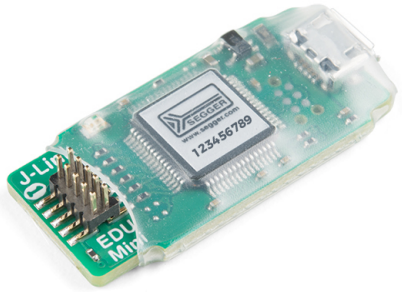

Figure 3.7: Segger J-Link Edu Mini. A Serial Wire Debug (SWD) probe used to flash the ATSAMD51 bootloader

As mentioned, PyCubed-Mini runs on CircuitPython firmware, enabling easy embedded programming through Python scripting. Adafruit has provided numerous guides on configuring, building, and flashing CircuitPython for a custom-designed board [16]. We offer compiled images of the PyCubed-Mini bootloader and firmware with our satellite design files.

Before flashing a bootloader on the cameraboard's STM32H7 microcontroller, we must activate its bootloader mode by pulling the BOOT0 pin high during power-on. A toggle switch on the cameraboard allows developers to select the appropriate mode during boot-up. Since our cameraboard is based on the OpenMV range of open-source camera modules, the OpenMV IDE can flash the STM32H7's bootloader, update its firmware, and program the cameraboard in Python directly via its USB port.

3.2.6 Battery Balancing

Before assembling the batteryboards, the two LiPo cells must have their voltages balanced. If cells with differing voltages are connected in parallel, the battery with the higher voltage will push current into the battery with the lower voltage. The magnitude of this reverse current is determined by the voltage difference between the two cells and the sum of their internal resistances. This tiny resistance, on the order of 10s of milliohms, may easily result in a reverse current that far exceeds the maximum recommended charging current of the individual cells. Such a high current may cause the batteries to overheat and potentially catch fire or explode.

To balance cell voltages, their negative terminals are tied together, while the positive terminals are connected to either end of a power resistor. This power resistor limits the maximum current flowing between the batteries. A fully charged battery (at 4.2V) and a fully discharged battery (at about 3.2V) would have a maximum potential difference of 1V between them. The value of the power resistor is chosen such that the current is limited to well below the maximum rated charge current. Additionally, the resistor should be capable of dissipating the heat generated within it due to that current. Higher resistances are thus safer, with the trade-off of prolonging the balancing process. An ammeter in series with the power resistor measures the current between the cells to estimate when the batteries are reasonably well balanced.

We developed a specialized power testing board with a microcontroller-monitored

battery balancing system. This board is an open-source testing device; we will discuss it in detail in the upcoming section.

3.2.7 Sealing the Satellite

Before conducting the final vibration test of the satellite prior to launch, a crucial step is to ensure a secure seal on the spacecraft. This sealing process involves carefully coating screws with Loctite and threaded standoffs during the satellite's final assembly. Doing so prevents any unintentional loosening of hardware due to the intense vibrations experienced during the test (and subsequently, during launch).

Disassembling the satellite would invalidate any previous vibration tests and require retesting the flight article to receive authorization for launch integration. Therefore, any hardware fixes must be performed prior to sealing.

The USB ports on the mainboard and cameraboard remain accessible through cutouts on the +Z solar panel, allowing software updates post-sealing.

3.3 Test Hardware and Procedures

As mentioned in the introduction to this thesis, satellite designs, especially those with custom hardware, require extensive testing and verification to ensure mission success. For this reason, one-third to one-half of the overall mission schedule should be allocated to integration, verification, and testing.

We have generated a list of tests that adequately verify the hardware design of our satellite. Whenever possible, we have devised testing apparatus to enhance our satellite development platform and simplify test development for end-users of our designs. These testing device designs keep with our goals of low cost, accessibility, and ease of use. This thesis section details the specific tests and their methodologies and showcases the dedicated hardware developed for relevant testing apparatus.

3.3.1 Power System Testing

Since PyCubed-Mini is a fully solar-powered satellite, any malfunction in its power system could rapidly lead to complete mission failure. Therefore, extensive power system testing is essential before the satellite can be considered viable for launch. The power system comprises multiple components that require verification individually and concurrently.

Solar Panel Verification

Since the satellite is typically delivered several months before launch, the batteries will likely be partially depleted at the start of the mission. As such, the solar panels must perform as expected to charge the batteries post-deployment.

A simple test for verifying solar panel functionality is to place the assembled satellite out in the sun and monitor the battery voltage over time. However, due to the unreliable sunlight in Pittsburgh, especially during the winter, we have developed an indoor solar testing platform using commercially available grow lights. These lights comprise a matrix of various wavelength LEDs in precise quantities to mimic the spectrum of sunlight.

We have also designed a specialized power tester board for verifying the components of PyCubed-Mini's power system (Figure 3.8). A newly assembled solar panel board is connected to the tester, and the apparatus is placed under grow lights. The solar panel is subjected to simulated constant current and constant power loads. This tester board integrates an RP2040 microcontroller that constantly monitors the parameters of solar panel current and voltage. Additionally, it utilizes the solar panel light sensor to determine the ambient light intensity. The microcontroller can verify whether the panel works within the expected parameters for the given light intensity.

Like the ATSAMD51 microcontroller on the satellite, the power tester board's RP2040 microcontroller runs CircuitPython. The RP2040 is popular among DIY electronics projects due to its low cost ($1 / piece) and stock availability. It interfaces with a 128x64 pixel OLED display that can optionally display a menu of tests or specific test parameters. A rotary encoder with an integrated switch is used to navigate the displayed menus.

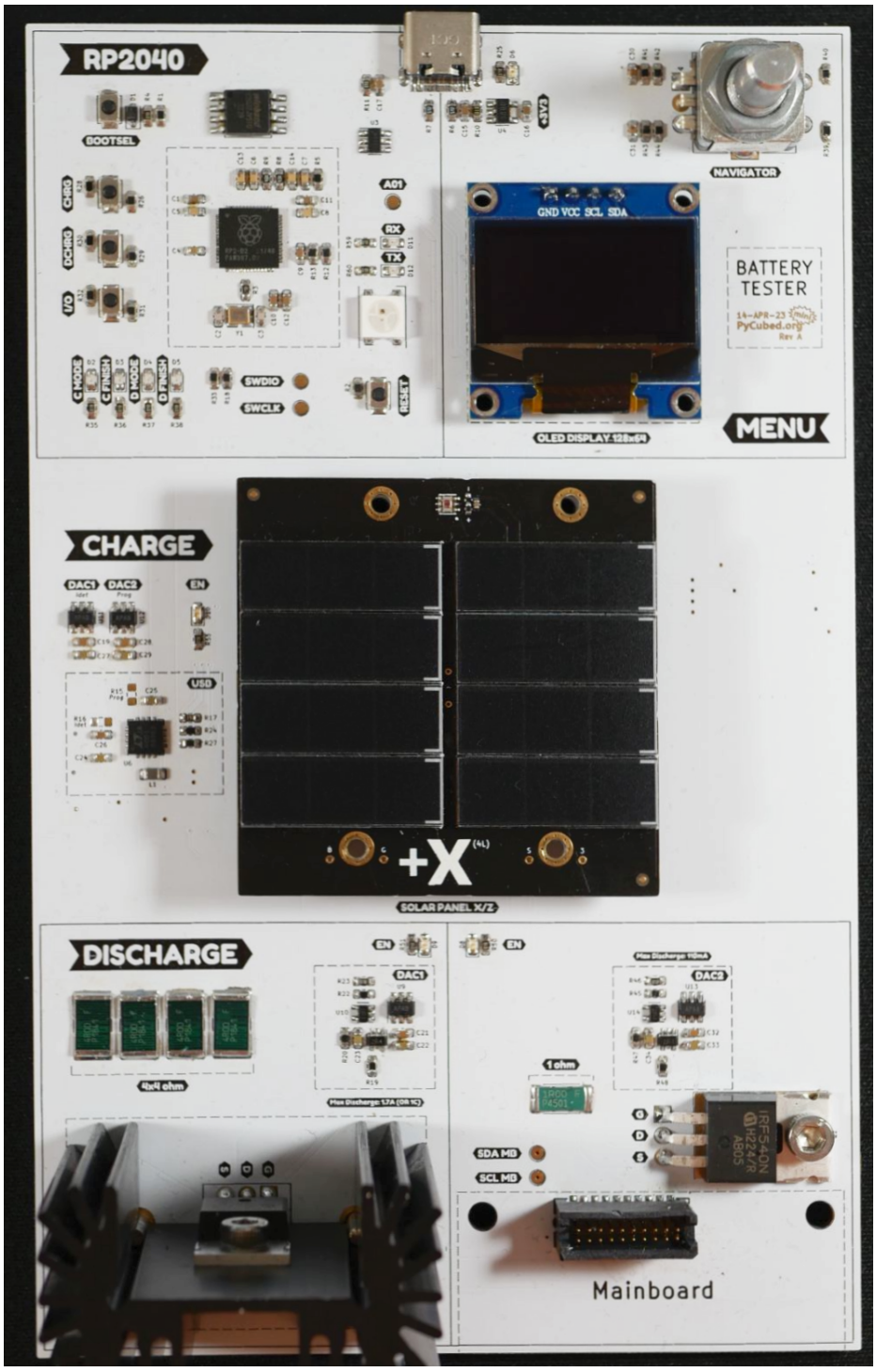

Figure 3.8: Power Tester Board: Front View - featuring RP2040 microcontroller (top-left), OLED display and a rotary encoder (top-right), battery charging circuit (middle-left), solar panel (middle), battery-discharge circuit (bottom-left), solar panel load circuit and mainboard attachment (bottom-right)

Battery Capacity Verification

It is a good idea to verify the power storage capacity of the LiPo cells before installing them into the satellite. Since the cells we use are COTS components, their actual capacity may differ from the manufacturer's rated capacity of 850mAh. Battery capacity may also vary significantly from one cell to another.

Lithium-polymer batteries have a non-linear relationship between their voltages and their discharge capacity (Figure 3.9). On our tester board, we use the MAX17048 fuel gauge IC by Analog Devices to estimate battery capacity. This I2C-controlled device performs the complex non-linear math required to estimate the charge level in the form of a percentage. Cells are connected to the tester board and undergo a series of automated charge/discharge cycles. Battery capacities are determined and plotted for varying charge/discharge rates, and the battery's health can be tracked over multiple cycles.

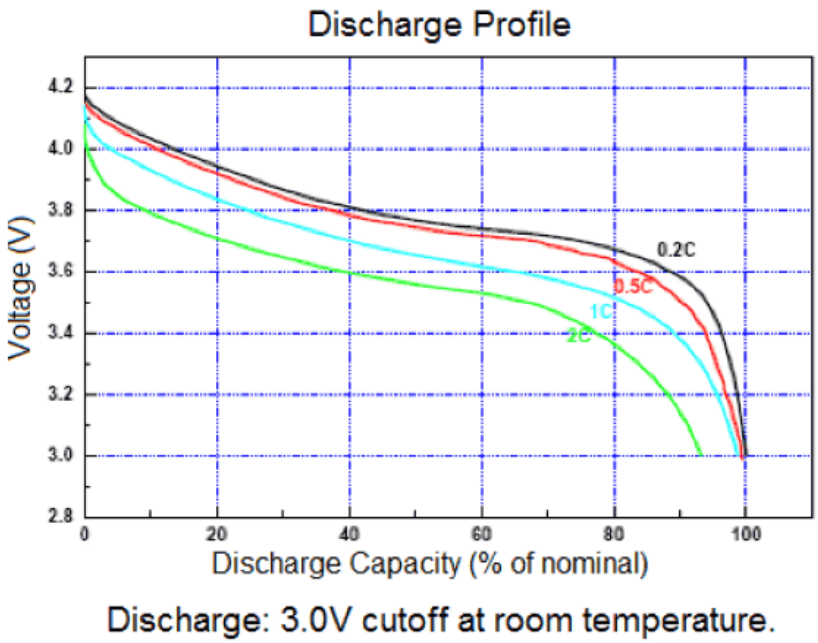

Figure 3.9: Typical LiPo battery discharge profile. *credit: Adafruit Industries*

A pair of cells that perform within spec is selected to be balanced and assembled onto a batteryboard. The assembled batteryboard with two cells connected in parallel is then subjected to its own series of charge/discharge tests.

Batteries undergo constant current and constant power charging. The LTC4001 battery charging IC by Analog Devices, used on the tester board, can set a maximum charge current of 2A, which allows testing the recommended 1C charge range of a 1.7 Ah batteryboard. The charge current of the IC is configurable by driving its PROG pin to a specific voltage via an MCP4725, 12-bit Digital-to-Analog converter (DAC). The RP2040 MCU can thus control the charge current over an I2C interface. By monitoring the battery voltage over time, we can implement constant power charging through software control of the charge current.

Batteries discharge through a unique Op-Amp and MOSFET circuit that utilizes a simple voltage-follower Op-Amp configuration (Figure 3.10). By setting the Op-Amp input voltage using a DAC, we can control the voltage difference across a 1-ohm resistor, resulting in the desired constant discharge current.

Again, by monitoring the battery voltage, the discharge current can be varied (through the DAC voltage) to test constant power loads.

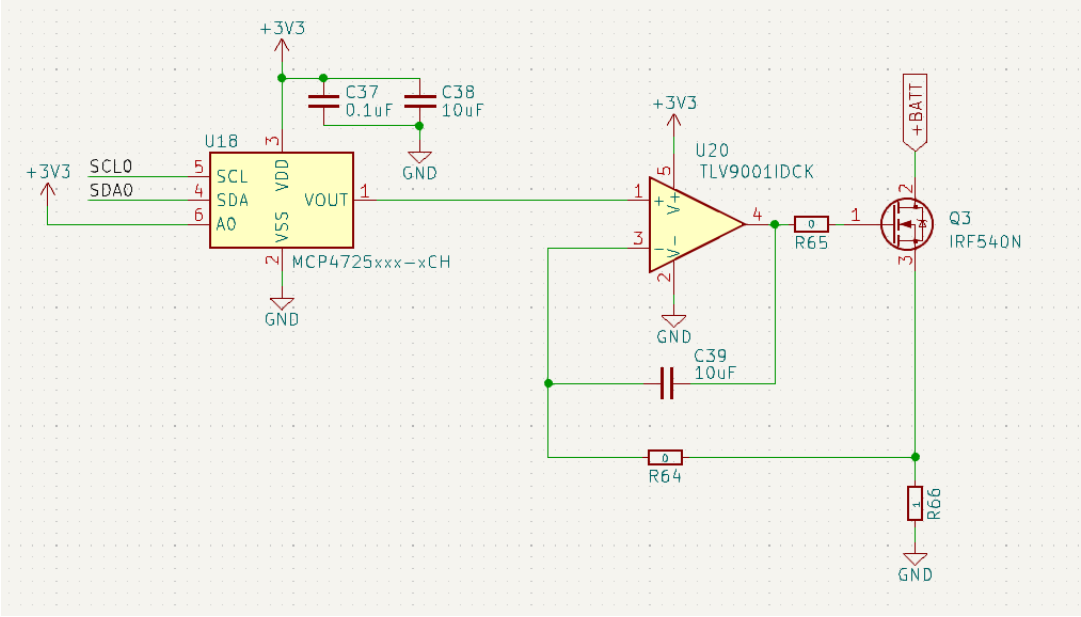

Figure 3.10: Op-Amp Battery Discharge Circuit [40]

The power from discharging the batteries converts to heat energy. A fully charged battery at 4.2V (V), discharging at the maximum recommended 1C constant current

(1.7A for the 1.7Ah batteryboard) (I), will generate,

$$P = VI = 4.2 \times 1.7 = 7.14W\ of\ heat$$

The power dissipated at the 1-ohm resistor is

$$P = I^2R = 1.7^2 \times 1 = 2.89W\ of\ heat$$

Thus the remaining 4.25W of heat is dissipated at the MOSFET.

To prevent the components in this circuit from overheating, we make design considerations to enable efficient heat dissipation. Instead of using a single 1-ohm resistor, we configure four 4-ohm SMD resistors in parallel (resulting in an equivalent resistance of 1 ohm), effectively increasing the surface area for heat dissipation by a factor of 4. The power MOSFET is mounted to an aluminum heatsink with a thermal resistance of 3.9 degrees Celsius / W, thus dissipating 4.25W of heat with a minor 16.6 degrees Celsius rise in temperature from ambient.

Other Features

The power tester board contains an automated battery balancing system. Unbalanced cells are connected in parallel across a power resistor, and the RP2040 MCU monitors the current between them. The balancing ends once the current falls beneath a configured threshold.

The mainboard or cameraboard (or both stacked together) may be connected to the tester board to serve as a satellite-accurate power load. Combined with a solar panel and batteryboard, this configuration is a close analog to PyCubed-Mini's complete power system. By varying light intensity, we can perform full-system verification and hardware-in-the-loop tests to develop our software power management system.

Figure 3.11: Power Tester Board: Back View - The batteries are mounted to the bottom of the tester boards to shield them from direct light. The boards are manufactured with a white solder mask to prevent overheating under the grow lights.

3.3.2 FlatSat-based Bench Testing

A FlatSat is an aerospace term used to describe a high-fidelity model of the spacecraft's entire hardware system, with individual components laid horizontally across a flat surface (as opposed to being in their closely integrated state). Appropriate connections between boards are made via cable harnesses or, in the case of a small spread of components like ours, using a PCB base.

The FlatSat allows us to keep the boards physically together in an electrically connected state and monitor any status LEDs on individual boards, probe test points, or utilize programming headers, which may be inaccessible in an assembled satellite. Boards may be individually connected, disconnected, or replaced with a different revision immediately without disassembling and reassembling the entire satellite.

We have designed a 2-layer PCB FlatSat for the PyCubed-Mini's circuit boards (Figure 3.12). The small size of our circuit boards enables the FlatSat to be relatively compact, reducing the cost of manufacture and easing the portability of the entire satellite infrastructure. The FlatSat has connectors and mechanical mounting holes for each circuit board and has traces laid out to connect the boards electrically.

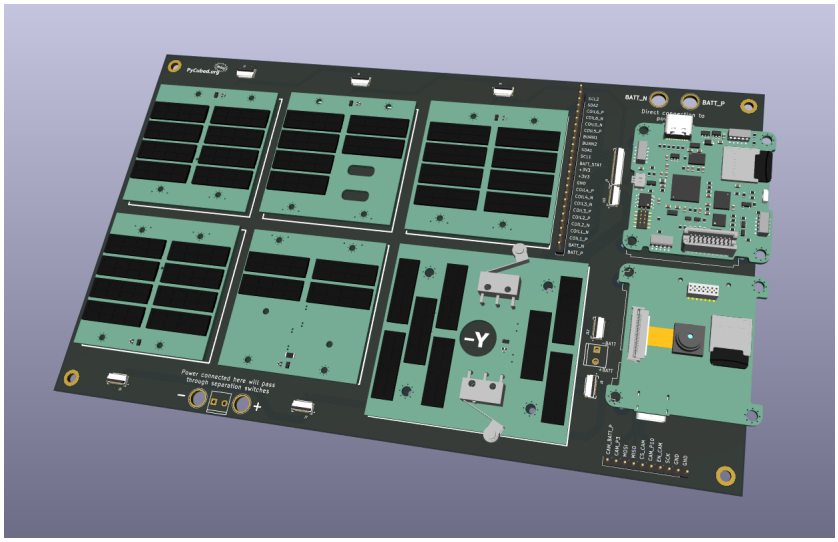

Figure 3.12: A model of PyCubed-Mini's FlatSat with all avionics PCBs integrated

The FlatSat finds the most use during initial board assembly. It enables modular system integration by assembling the avionics architecture one board at a time,

testing each newly added board. For example, it allows us to verify whether a newly assembled mainboard or cameraboard can be flashed correctly, switch between battery and USB power as required, detect and read all its sensors, and verify the accuracy of their data. Sensors like the IMU can be verified by physically rotating the FlatSat and observing the generated roll, pitch, and yaw angles. If any hardware issues are identified, required repairs can be performed, and the board can be reintegrated into the avionics immediately.

The FlatSat allows effective power and data interface testing between the mainboard and cameraboard. The cameraboard mounts to the FlatSat with its camera module pointed upwards, allowing us to take useful images. The FlatSat provides direct access to the micro-SD cards on both the mainboard and cameraboard, which become inaccessible on an assembled satellite. Any data stored on the cards, such as high-resolution images or CV algorithm data products, can be accessed quickly by plugging them into an external computer.

The entire FlatSat is small enough to fit under our grow light setup, enabling us to test the solar charging system with all the solar panels connected. In such a configuration, all the light sensors on the solar panels should provide similar light readings, so any malfunctioning light sensors would be easy to detect.

3.3.3 Attitude Determination and Control Hardware-in-the-Loop Testbed

PyCubed-Mini's attitude determination and control system (ADCS) is crucial to make productive use of its vision system by being able to point the satellite's camera toward the features on Earth we would like to observe.

PyCubed-Mini relies on simple consumer-grade magnetometers, gyroscopes, and sun sensors to estimate the satellite's orientation and implements a magnetorquer-only attitude control system. Sophisticated calibration, motion planning, and control software enhance the effectiveness of this system. As a result, we can achieve complete three-axis attitude determination and control. The system is also completely solid-state, with no moving parts or need for consumable propellant, significantly reducing the chance of hardware failure.

We extend the work by Jensen and Manchester (2022) [27] to develop an open-

source hardware-in-the-loop simulator to enable rapid testing of a PocketQube satellite's magnetorquer ADCS hardware and software. The tester can measure the satellite's magnetorquer response and use it to simulate its attitude control.

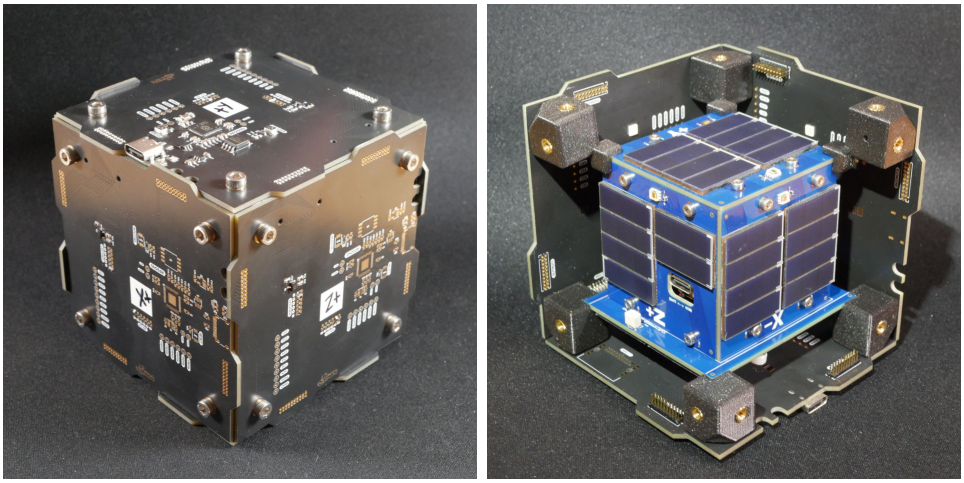

Figure 3.13: ADCS Hardware-in-the-Loop testbed. Closed view (left), open-view to show the placement of PyCubed-Mini inside (right)

The ADCS simulator is an 8 cm × 8 cm × 8 cm cube-shaped testbed. Printed circuit boards used for the faces connect via right-angled pin headers that route power, data, and I/O lines between boards. The boards screw into threaded heat inserts installed on 3D-printed corner pieces for increased mechanical stability. Four corner pieces form a base for the PocketQube to sit on inside the tester, sized such that they position the satellite equidistant from each face (Right image in Figure 3.13). The four remaining corner pieces securely hold the satellite inside the box when fully assembled. The satellite can be monitored in real-time by connecting it to an external computer via USB cables.

The simulator is designed with six identical PCBs to reduce manufacturing costs. This single design is achieved by merging every possible configuration of components onto a single design and then selectively populating only the components required on a specific face. For example, just one board must be populated with an RP2040 microcontroller, associated circuitry, and a USB-C connector. The PCB has been routed such that components on all six boards can be interfaced regardless of which face is populated with the microcontroller. Like the satellite's primary MCU and the

RP2040 on the power tester board, this microcontroller runs CircuitPython firmware for simple Python-based test programming.

Each board features a LIS3MDL magnetometer by STMicroelectronics positioned at the center of the inner face of the boards. Wiring these via an SPI interface allows us to place all six magnetometers on the same serial bus. Chip Select (CS) lines determine which specific component on the SPI bus is being communicated with by the host. Six CS lines are routed from the RP2040 microcontroller to each face of the device. A unique CS line is connected to each magnetometer by populating a 0-ohm resistor between the magnetometer and that CS line.

Furthermore, each board has eight mounting pads for LEDs. These are arranged such that one will always be directly over the light sensor on each solar panel. Only that LED is populated on the respective boards. We used full-spectrum LEDs from Wurth Elektronik with a spectral emission close to the sun. These LEDs are driven via a PWM-MOSFET circuit, allowing full brightness control. Like the CS lines on the magnetometer, six PWM lines are routed from the microcontroller, and a unique PWM line is connected to the MOSFET circuit on each board by populating a 0-ohm resistor.

We utilize the methods outlined by Jensen and Manchester [27] to calibrate the magnetometers and light sensors prior to usage. In order to test the attitude determination and control system, the magnetorquer coils on the PocketQube are selectively powered to generate a magnetic dipole. The magnetometers on each axis of the box can measure the strength of this dipole. We can simulate a sun vector by illuminating specific LEDs and adjusting their brightness. The magnetic fields generated by the magnetorquer coils on each axis are fed into the simulator dynamics, and the sun vector is altered in response. This allows us to simulate the magnetic torque's effect on the satellite's attitude without having to move any hardware physically.

We are working towards integrating 3-axis Helmholtz coils for the ADCS testbed to allow us to simulate arbitrary environmental magnetic fields and improve the fidelity of our satellite ADCS hardware-in-the-loop simulation.

3.3.4 Ground Station and Range Testing

PyCubed-Mini's comms form just one-half of the communication link between the satellite and Earth. A ground or terrestrial radio station enables extra-planetary telecommunication with spacecraft. As part of our satellite development platform, we have built a low-cost, easy-to-use ground station hardware and software package. We have used our custom ground station to conduct long-range communication tests and intend to use it to communicate with the satellite once it is in orbit.

The ground station is based on the popular Raspberry Pi range of single-board computers (SBCs). We attach a custom-designed daughterboard for radio communications in the standard HAT form factor. This board interfaces with the Raspberry Pi via its 40-pin GPIO header. The radio HAT integrates two RFM98PW modules - the same radio used on board the satellite - to establish two communication channels capable of transmission (TX) and reception (RX). The Raspberry Pi host manages the radio modules via an SPI interface.

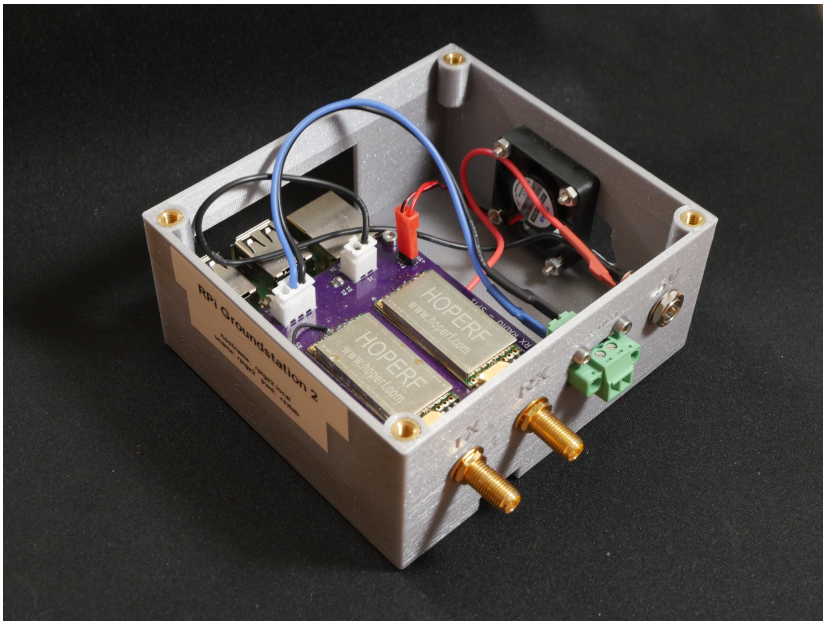

Figure 3.14: Raspberry Pi-based ground station with custom radio HAT

In order to test the satellite's communication system, two teams, one with the satellite and the other with the grounds station and antenna, are positioned at a distance of 1km away from each other - at locations with clear line-of-sight. We have

written automated radio testing scripts in Python that run simultaneously on both the satellite and the ground station. Data is transmitted by the ground station and received by the satellite and then, in turn, transmitted by the satellite and received by the ground station. The scripts verify whether the received data is identical to what was sent initially. Then the process is reversed, with the satellite transmitting first.

About 60dB of attenuation is added in line with the ground station antenna to mimic a 1000km satellite altitude. We have successfully tested PyCubed-Mini's communication system with this configuration.

Figure 3.15: Photographs from a long-distance satellite communication test. PyCubed-Mini (left), ground station and antenna (right)

Chapter 4

Conclusions

We eagerly look forward to two upcoming PyCubed-Mini launches in the Fall of 2023. This mission will primarily serve to test PyCubed-Mini's attitude determination and control system (ADCS) and the performance of magnetorquer-only attitude control on a PocketQube scale satellite - an implementation of the work by Gatherer and Manchester [14]. We intend to use PyCubed-Mini's attitude control ability for Earth observation and imaging and to implement preliminary onboard computer vision processing. Furthermore, we would like to stress-test the satellite's communication systems by attempting remote software updates, and transmitting large data products (such as high-resolution imagery) within limited bandwidth, using fountain code-based data packetization. A space mission will be the ultimate test of our work so far.

Gaining space heritage would establish PyCubed-Mini as a worthy platform upon which other universities may base their missions. While we are confident of the quality of our current flight designs, we have planned improvements to add features, improve functionality, simplify manufacture, and reduce costs. We discuss these in the final section of this thesis.

4.0.1 Future Work

Structural Design

To start, let us discuss potential future improvements to the structural design. As discussed in its dedicated design section, typical 3D-printing filaments such as PLA

are unsuitable for space missions due to their high out-gassing, low melting points, and poor mechanical characteristics. Thus, we have been utilizing a specialized carbon-fiber reinforced composite Windform XT 2.0, which comes at a significant cost and extended lead time. We intend to search for low-cost materials that can be used in ordinary 3D printers while exhibiting our desired low out-gassing and thermal and mechanical properties. We would also like to explore the effect of the bake-out process on the levels of out-gassing from common filaments. Being able to fully manufacture the satellite's hardware in-house would be a significant step towards our mission of a low-cost, effectively-DIY satellite platform.

Furthermore, from experience gained through building several prototype satellite assemblies, we have discovered that installing threaded heat inserts into the plastic of the rails, using a hand-held soldering iron, can cause the plastic to warp and deform quite easily. Furthermore, it may result in off-angle installations, which may affect not just the ease of assembly but also the mechanical integrity of the satellite. To address this, we aim to design and assemble a simple jig to steady the soldering iron and 3D-printed components during installation.

Power System

Most of our planned satellite design improvements focus on its power system.

The LiPo cells we currently use employ an onboard protection circuit PCB. An option would be to use raw cells with no such circuitry, which may allow us to fit cells of greater capacity within the volume of our satellite. The battery protection circuitry could then be integrated into the EPS board. We have avoided this avenue due to the inherent dangers of working with bare LiPo cells, especially for beginners. We will also look towards single battery solutions to remove the need to balance cell voltages prior to installation.

The solar cells currently constitute the most expensive component of our satellite at about $125. Our ultimate goal is for an entire PyCubed-Mini satellite to cost the same as a single 1U PyCubed mainboard — approximately $250. In future designs, we will explore a configuration of fewer but larger solar cells that will lower overall component costs while increasing our power generation capability. We have specced the SM141K05L solar cells by AnySolar, which in a 2-parallel (2p) configuration per

solar panel, would cost a total of $70 (a 44% decrease) and would additionally improve our per panel max power production from 245.6mW to 308mW, a 25% increase.

We additionally intend to redesign the power harvesting system to lower redundancy and cost while maintaining (or improving) our current efficiency. Instead of requiring a unique energy harvesting circuit for each solar panel board, a single circuit will integrate into a future revision of the EPS board, which will further simplify the solar panel design.

In our current design, once installed, the batteries may only be charged externally through a DC power supply directly connected to the battery terminals through a connector on the -Y solar panel. This configuration is not ideal as it requires constant monitoring of the DC power supply to avoid an over-charge or over-current scenario, besides being generally tedious. In a future update to the EPS board, we would like to integrate a USB charging circuit with a dedicated PMIC (Power Management Integrated Circuit) that can safely charge the batteries and stop charging once the batteries are at full capacity.

Other features for the EPS board on the bucket list include voltage regulation, active power monitoring, and load switches - which would allow us to implement multiple power levels on the satellite, wherein only specific components are turned on depending on the available power budget.

Avionics Design and Computation System

Our satellite has a few mission-critical components lacking any radiation performance data or space heritage: the BNO085 IMU, PCF8523 RTC, DRV8830 coil drivers, and the BQ25570 PMICs. Since the failure of these components could mean a loss of some or all of our mission objectives, we would like to conduct radiation testing on them. Furthermore, we would like to compile a list of commonly used COTS components with thorough radiation performance data.

Currently, we need a slightly different solar panel design for each face of the satellite (except the +X and -X boards). This results in increased PCB manufacturing costs. A planned update is to use the same solar panel design for the X and Z boards, which would additionally increase total power generation and improve the aesthetics of our satellite. Unfortunately, the drawbacks here would be a required redesign

of the antenna board and loss of access to the USB ports on the mainboard and cameraboard.

We could route the USB power and data lines down the stack connector; however, we have limited available pins on the current satellite bus. We have an idea of establishing a standard for the PocketQube PCB layout similar to the PC/104 standard for CubeSats. The PC/104 standard is called so because of the 104 pins on the PCB bus connectors. If we laid out two pin header connectors on either side of the board, this would double bus pins from 20 to 40 but require a significant redesign of all the stack boards.

Communications design

In aid of using the same board design for the X and Z board panels, the antennas could be moved to the +Y or -Y solar panels. Due to the difference in physical dimensions, these boards require a unique design in any scenario.

We also intend to explore creating a custom radio board, allowing us to easily reconfigure the satellite comms to a wide range of frequency bands and amplify the transmission power beyond the +30dBm of our radio modules. Additionally, it would help free up space on the currently cramped mainboard.

Vision system

We intend to explore other camera modules with different resolutions and optical parameters. We also wish to explore the kinds of unique computer vision applications for which our satellite may be useful.

Thermal system

A classical spacecraft system we have not yet discussed is the thermal system. Satellites typically run cool in space, so a simple consideration to warm them up is to select a dark color for the solar panel PCB solder mask. Batteries are susceptible to low temperatures and may have their capacities reduced or refuse to charge altogether. We currently do not implement any method of actively heating the batteries if their temperatures drop below the recommended operating range. We intend to remedy this in the future as well.

Documentation and Accessibility

Finally, our project will only achieve its goal of serving as a platform for other universities to base their missions if they are aware of its existence and can easily and quickly acquire the information they would need to build a PyCubed-Mini satellite themselves. We aim to document all our designs and manufacturing procedures extensively, with step-by-step guides for assembly, integration, and testing.

Appendix A

List of Acronyms and Abbreviations

ADC	Analog-to-Digital Converter
ADCS	Attitude Determination and Control System
AEC	Automotive Electronics Council
ALS	Ambient Light Sensor
CNC	Computer Numerical Control
COTS	Commercial Off The Shelf
CS	Chip Select
CTE	Coefficient of Thermal Expansion
CV	Computer Vision
DAC	Digital-to-Analog Converter
DC	Direct Current
DIY	Do It Yourself
DoF	Degrees of Freedom
DVP	Digital Video Port
EMI	Electromagnetic Interference
ENIG	Electroless Nickel Immersion Gold
EPS	Electrical Power Systems
ESA	European Space Agency
ESD	Electrostatic Discharge

FAA	Federal Aviation Administration
FFC	Flat-Flex Connector
FOV	Field Of View
FPGA	Field Programmable Gate Array
FSK	Frequency-Shift Keying
GFSK	Gaussian Frequency-Shift Keying
GMSK	Gaussian Minimum-Shift Keying
GNC	Guidance, Navigation, and Control
GPS	Global Positioning System
HEO	High Earth Orbit
I2C	Inter-Integrated Circuit
IC	Integrated Circuit
IDE	Integrated Development Environment
IMU	Inertial Measurement Unit
I/O	Input / Output
IPC	Institute of Printed Circuits
ISM	Industrial, Scientific, and Medical
ITAR	International Traffic in Arms Regulations
IoT	Internet of Things
LDO	Low Dropout
LED	Light Emitting Diode
LEO	Low Earth Orbit
LiPo	Lithium Polymer
LoRa	Long Range
LQR	Linear–Quadratic Regulator
M2M	Machine-to-Machine
MCU	Microcontroller Unit
MEO	Medium Earth Orbit
MLC	Multi-Level Cells
MOSFET	Metal-Oxide-Semiconductor Field Effect Transistor
MP	Mega Pixels = 1,000,000 Pixels
MPP	Maximum Peak Power
MPPT	Maximum Power Point Tracking
MRAM	Magnetoresistive Random-Access Memory

MSK	Minimum-Shift Keying
NASA	National Aeronautics and Space Administration
OLED	Organic Light Emitting Diode
OOK	On–Off Keying
Op-Amp	Operational Amplifier
PCB	Printed Circuit Board
PLA	Polylactic Acid, a type of common 3D-printing filament
PMIC	Power Management Integrated Circuit
PTH	Plated-Through Holes
PV	Photovoltaic
PWM	Pulse Width Modulation
QFN	Quad Flat No-lead
QSPI	Quad Serial Peripheral Interface
RCS	Reaction Control System
RExLab	Robot Exploration Lab at Carnegie Mellon University
RF	Radio Frequency
RTC	Real Time Clock
RX	Receive, Receiver, or Reception
SBC	Single Board Computer
SCCB	Serial Camera Control Bus
SERCOM	Serial Communication
SEU	Single Event Upset
SLC	Single-Level Cells
SMD	Surface-Mount Device
SPI	Serial Peripheral Interface
SWD	Serial Wire Debug
Tg	Glass-transition Temperature
TI	Texas Instruments
TID	Total Ionizing Dose
TX	Transmit, Transmitter, or Transmission
UART	Universal Asynchronous Receiver / Transmitter
USB	Universal Serial Bus
VNA	Vector Network Analyzer
WDT	Watchdog Timer

Bibliography

[1] Anita Bernie, Paul Madle, Jamie Bayley, John Paffett, Keith Ryden, Benjamin Clewer, Alex Hands, and Chris Bridges. Results from Testing Low-Cost, High-Performance Terrestrial Processors for Use in Low-Cost High-Performance Space Missions. *35th Annual Small Satellite Conference*, 2021. 2.6.2

[2] Lucinda Berthoud, Michael Swartwout, James Cutler, David Klumpar, Jesper A. Larsen, and Jens Dalsgaard Nielsen. University CubeSat Project Management for Success. *33rd Annual AIAA/USU Conference on Small Satellites*, 2019. 1.2

[3] Donna J Cochran, Stephen P Buchner, Anthony B Sanders, Kenneth A LaBel, Martin A Carts, Christian F Poivey, Timothy R Oldham, Ray L Ladbury, Martha V O'Bryan, and Susan R Mackey. Compendium of recent total ionizing dose results for candidate spacecraft electronics for NASA. In *2008 IEEE Radiation Effects Data Workshop*, volume 510. IEEE, 2008. 2.3.2

[4] Lloyd W Condra, Stephan J Meschter, David A Pinsky, and Anthony J Rafanelli. The challenge of lead-free electronics for aerospace electronic systems. In *2009 IEEE Custom Integrated Circuits Conference*, pages 355–362. IEEE, 2009. 3.2.3

[5] PC/104 Consortium. PC/104 Specification, 2008. URL https://pc104.org/hardware-specifications/pc104/. 2.1.3

[6] Semtech Corporation. AN1200.22: LoRa Modulation Basics, 2015. URL https://web.archive.org/web/20190718200516/https://www.semtech.com/uploads/documents/an1200.22.pdf. Archived from the original 18 July 2019. Retrieved 8 August 2023. 2.4.1

[7] Roger Devaney. Solder Joint & Interconnect Technology and Failure Analysis. Technical report, Hi-Rel Laboratories, 2015. (document), 3.2

[8] Analog Devices. Cut Your Losses—With an Ideal Diode, 2017. URL https://www.maximintegrated.com/content/dam/files/design/technical-documents/design-solutions/ds50-cut-your-losses-with-an-ideal-diode.pdf. 2.2.4

[9] Analog Devices. MAX706: Low-Cost, µP Supervisory Circuits, 2018. URL https://www.analog.com/en/products/max706.html. 2.3.2

[10] Analog Devices. LTC4412: Low Loss PowerPath™ Controller in ThinSOT, 2020. URL https://www.analog.com/en/products/ltc4412.html. (document), 2.2.5, 2.19

[11] Analog Devices. MAX40200: Ultra-Tiny Micropower, 1A Ideal Diode with Ultra-Low Voltage Drop, 2023. URL https://www.analog.com/en/products/max40200.html. 2.2.4

[12] DigiKey. KXOB25-05X3F-TR. URL https://www.digikey.com/en/products/detail/anysolar-ltd/KXOB25-05X3F-TR/9990478. Accessed 08 August 2023. 2.2.1

[13] Federal Aviation Administration (FAA). The Annual Compendium of Commercial Space Transportation, 2018. URL https://www.faa.gov/about/office_org/headquarters_offices/ast/media/2018_ast_compendium.pdf. (document), 1.1, 1.1

[14] Andrew Gatherer and Zac Manchester. Magnetorquer-only attitude control of small satellites using trajectory optimization. In *Proceedings of AAS/AIAA Astrodynamics Specialist Conference*, 2019. 2.5.2, 4

[15] Isolar Group. FR408HR: High Performance Laminate and Prepreg, 2023. URL https://www.isola-group.com/pcb-laminates-prepreg/fr408hr-laminate-and-prepreg/. 3.1.2

[16] Dan Halbert. Building CircuitPython, 2023. URL https://learn.adafruit.com/building-circuitpython/introduction. 3.2.5

[17] Max Holliday, Kevin Tracy, Zachary Manchester, and Anh Nguyen. The V-R3X mission: Towards autonomous networking and navigation for Cubesat swarms. *The 4S Symposium*, 2022. 2.3.1

[18] Maximillian Holliday, Andrea Ramirez, Connor Settle, Tane Tatum, Debbie Senesky, and Zachary Manchester. Pycubed: An open-source, radiation-tested cubesat platform programmable entirely in python. *33rd Annual AIAA/USU Conference on Small Satellites*, 2019. 2.3.1, 2.3.1, 2.3.2, 3.1.2

[19] Maximillian Holliday, Zachary Manchester, and Debbie G Senesky. On-orbit implementation of discrete isolation schemes for improved reliability of serial communication buses. *IEEE Transactions on Aerospace and Electronic Systems*, 58(4):2973–2982, 2022. (document), 2.35, 2.7, 2.36

[20] HopeRF. RFM98PW: Enhanced Power Long Range Transceiver Module, 2006. URL https://www.hoperf.com/modules/lora/RFM98P.html. 2.3.2, 2.4.1

[21] Microchip Technology Inc. ATSAMD51J19A (datasheet), 2023. URL https://www.microchip.com/en-us/product/atsamd51j19a. 2.3.2

[22] Texas Instruments. DRV8830: Low-Voltage Motor Driver With Serial Interface,

2015. URL https://www.ti.com/product/DRV8830. 2.3.2

[23] Texas Instruments. INA219 Zerø-Drift, Bidirectional Current/Power Monitor With I2C Interface, 2015. URL https://www.ti.com/product/INA219. 2.2.6

[24] Texas Instruments. BQ25570: Ultra Low power Harvester power Management IC with boost charger, and Nanopower Buck Converter, 2019. URL https://www.ti.com/product/BQ25570. 2.2.2, 2.2.4

[25] Texas Instruments. OPT4001: High-speed high-precision digital ambient light sensor (ALS), 2022. URL https://www.ti.com/product/OPT4001. 2.5.1

[26] Farokh Irom and Gregory R Allen. Radiation tests of highly scaled, high-density, commercial, nonvolatile nand flash memories-update 2012. Technical report, Jet Propulsion Laboratory, 2012. 2.3.2

[27] Benjamin Jensen and Zachary Manchester. A Low-Cost Attitude Determination and Control System and Hardware-in-the-Loop Testbed for CubeSats. *36th Annual Small Satellite Conference*, 2022. 3.3.3, 3.3.3

[28] Aaron J Kenna, Bernard G Rax, Dennis O Thorbourn, Richard D Harris, and Steven S McClure. Compendium of recent total ionizing dose test results conducted by the jet propulsion laboratory from 2003 through 2009. In *2009 IEEE Radiation Effects Data Workshop*, pages 32–38. IEEE, 2009. 2.3.2

[29] Randy Kong, Cheryl Tulkoff, Craig Hillman, and DfR Solutions. The reliability challenges of qfn packaging. In *SMTA China East Conference*, 2010. 3.2.1

[30] Erik Kulu. Nanosats Database, 2023. URL https://www.nanosats.eu/. Accessed 8 August 2023. 1.1, 1.3

[31] Aekjira Kuyyakanont, Suwat Kuntanapreeda, and Nisai H Fuengwarodsakul. On verifying magnetic dipole moment of a magnetic torquer by experiments. In *IOP Conference Series: Materials Science and Engineering*, volume 297. IOP Publishing, 2018. (document), 2.29

[32] Andreas Larsson. *Die-attach for high-temperature electronics*. PhD thesis, University of South-Eastern Norway, 2019. (document), 3.5

[33] NASA. State-of-the-Art of Small Spacecraft Technology, 2022. URL https://www.nasa.gov/smallsat-institute/sst-soa/structures-materials-and-mechanisms. 6.0 Structures, Materials, and Mechanisms. 2.1.1

[34] Alba Orbital. PocketQube Kit v1.0 EM, 2023. URL https://www.albaorbital.com/hardware/pocketqube-kit. (document), 2.1.1, 2.3

[35] Alba Orbital. Solar Panels 1p Set, 2023. URL https://www.albaorbital.com/hardware/solar-panels-1p-set-qty-5. 2.2.1

[36] Alba Orbital, Delft University of Technology, and GAUSS Srl. The PocketQube

Standard, 2018. URL https://www.albaorbital.com/pocketqube-standard. (document), 1.3, 2.1

[37] Zachariah Peterson. The Digital Engineer's Guide to RF PCB Design Guidelines: Layout and Routing, 2021. URL https://resources.altium.com/p/digital-engineers-guide-rf-pcb-layout-and-routing. 2.4.1

[38] Michael Sampson, Henning Leidecker, Lyudmyla Panashchenko, Jay Brusse, and Jong Kim. Tin (and Other Metal) Whisker Induced Failures, 2009. URL https://nepp.nasa.gov/WHISKER/failures/index.htm. 3.2.3

[39] SatCatalog. CubeSat Launch Costs, 2022. URL https://www.satcatalog.com/insights/cubesat-launch-costs/. 1.2.1

[40] Garrett Satterfield. Programmable low-side current sink circuit. Technical report, Texas Instruments, 2018. (document), 3.10

[41] NXP Semiconductors. PCF8523: Real-Time Clock (RTC) and calendar, 2015. URL https://www.nxp.com/docs/en/data-sheet/PCF8523.pdf. 2.3.2

[42] Doug Sinclair and Jonathan Dyer. Radiation effects and COTS parts in SmallSats. *27th Annual AIAA/USU Conference on Small Satellites*, 2013. 2.3.1

[43] CEVA Technologies. BNO08X 9-axis IMU, 2023. URL https://www.ceva-dsp.com/product/bno-9-axis-imu/. 2.3.2

[44] CRP Technology. Windform Laser Sintering materials have passed outgassing screening at NASA, 2013. URL https://www.windform.com/news/windform-sls-materials-passed-outgassing-screening-nasa/. 3.1.1

[45] CRP Technology. New achievements for Windform materials, 2015. URL https://www.windform.com/news/new-achievements-windform-materials/. 3.1.1

[46] CRP Technology. 3D printed satellite deployer in Windform XT 2.0 acclaimed, 2020. URL https://www.crptechnology.com/news/3d-printed-satellite-deployer-windform-xt-2-0-acclaimed/. 3.1.1

[47] CRP Technology. 3D printed satellite, how CRP USA and Windform LX 3.0 composite helped PSAS's OreSat0 CubeSat get to orbit, 2021. URL https://www.windform.com/case-studies/3d-printed-satellite-oresat0-3d-printed-parts-subsystems/. 3.1.1

[48] Paul Mark Thelen. Introduction to the Space Radiation Environment, 6 2018. URL https://www.osti.gov/biblio/1524958. 2.3.1

[49] Robert J. Twiggs. Making it Small, 2009. URL https://web.archive.org/web/20160303185449/http://mstl.atl.calpoly.edu/~bklofas/Presentations/DevelopersWorkshop2009/7_CubeSat_Alt/1_Twiggs-PocketQub.pdf. Archived from the original 3 March 2016. Retrieved 8 August 2023. 1.3

[50] California Polytechnic State University. CubeSat Design Specification Rev. 14.1, 2022. URL https://www.cubesat.org/s/CDS-REV14_1-2022-02-09.pdf. 1.1

[51] Isabellenhuette USA. ISA-PLAN® / Precision Resistors, 2019. URL https://www.isabellenhuetteusa.com/?product=sms. 2.2.6

[52] Catherine Venturini, Barbara Braun, David Hinkley, and Greg Berg. Improving Mission Success of CubeSats. *32nd Annual AIAA/USU Conference on Small Satellites*, 2018. 1.2.4

[53] Wikipedia. 2020–2023 global chip shortage, 2023. URL https://en.wikipedia.org/wiki/2020-2023_global_chip_shortage. Accessed 08 August 2023. 2.3.1

[54] Wikipedia. Maximum power point tracking, 2023. URL https://en.wikipedia.org/wiki/Maximum_power_point_tracking. Accessed 08 August 2023. (document), 2.2.2, 2.13